



Covenant Journal of Engineering Technology (CJET)

Vol. 1 No. 2, Dec. 2017

**A Bi-annual publication of the College of Engineering,
Covenant University, Canaanland.
Km 10, Idiroko Road, Ota, Ogun State, Nigeria.**

Editor-in-Chief: Dr. Charles Ndujube
editorcjjet@covenantuniversity.edu.ng

Managing Editor: Edwin O. Agbaike
me@covenantuniversity.edu.ng

Website: <http://Journal.covenantuniversity.edu.ng/cjet/>

© 2017, Covenant University Journals

All rights reserved. No part of this publication may be reproduced, stored in a retrieval system or transmitted in any form or by any means, electronic, electrostatic, magnetic tape, mechanical, photocopying, recording or otherwise, without the prior written permission of the publisher.

It is a condition of publication in this journal that manuscripts have not been published or submitted for publication and will not be submitted or published elsewhere.

Upon the acceptance of articles to be published in this journal, the author(s) are required to transfer copyright of the article to the publisher.

ISSN: Print xxxx-xxxx
 Online xxxx-xxxx

Published by Covenant University Journals,
Covenant University, Canaanland, Km 10, Idiroko Road,
P.M.B. 1023, Ota, Ogun State, Nigeria

Printed by Covenant University Press

Articles

Optimization of Atmospheric Distillation Unit of Warri Refinery using Artificial Neural Network and Exergy Rate Profiles Funmilayo N. Osulale & Ambrose N. Anozie	1
Assessment of Pre-Stressed Concrete Electric Poles for Rural Electrification Projects Adegboyega G. A. & Adewuyi P. A.	16
Comparative Study of the use of Arithmetic Mean and Geometric Mean for Data Aggregation in FMEA Analysis Ikuobase Emovon & Modestus Okechukwu Okwu	24
Crevice Corrosion Behaviour of Nickel-Based alloy 718 in both Aerated and De-Aerated Chloride Environment F. Bakare, J. Ugorji, Y. Alsubhi, S. Okunzuwa & A.Orobor	40
Suitability of some Selected Ado-Ekiti (Nigeria) Natural Moulding Sands' Properties for Sand Casting Shuaib-Babata Y. L., Yaru S.S., Abdulkareem S., Ajayi S., Busari Y. O., Ajao K. S., Ibrahim H. K., Ambali I. O & Mohammed G. A.	53
Development of an Encrypting System for an Image Viewer based on Hill Cipher Algorithm Okereke Chinonso, Osemwegie Omoruyi, Kennedy Okokpujie & Samuel John	65
Evaluation of Blends of Agricultural Solid Biomass Waste for Solid Fuel Production Augustine O. Ayeni, David O. Odede, Ayodeji Ayoola, Opeyemi Adeeyo & Ajibola Ogunbiyi	74



Optimization of Atmospheric Distillation Unit of Warri Refinery Using Artificial Neural Network and Exergy Rate Profiles

Funmilayo N. Osuolale^{1*} & Ambrose N. Anozie²

¹Ladoke Akintola University of Technology,
Ogbomoso, Oyo State, Nigeria
fnosuolale@lautech.edu.ng

²Covenant University,
Ota, Ogun State, Nigeria
ambrose.anozie@covenantuniversity.edu.ng

*Correspondence: fnosuolale@lautech.edu.ng

Abstract: In this paper, the operation of atmospheric distillation unit (ADU) of Warri refinery was optimized using Artificial Neural Network (ANN) method of optimization and exergy rate profiles (ERP). Optimization of ADU exergy efficiency using nine operating variables and ANN method of optimization improved exergy efficiency from 33% to 53%. The vapour and liquid exergy rate profiles in the distillation column were used to reveal points of inefficiency within the column and as a retrofit tool to suggest possible column modification alternatives for energy efficient operations. The exergy rate profiles in the column were found to be crossing each other. Optimization of the ADU when the crossing of the exergy rate profiles in the column was removed further improved ADU exergy efficiency from 53% to 60%. Artificial neural network was shown to be a powerful and suitable optimization method for solving constrained optimization problems such as in atmospheric distillation unit with several operating variables with constraints. Exergy rate profiles depict the driving forces between the liquid and the vapour states in a column and were shown to be a suitable tool for further improvement of ADU exergy efficiency.

Keywords: Atmospheric Distillation Unit; Artificial neural network; Exergy efficiency; Optimization; Exergy rate profiles

1. Introduction

Distillation process contrary to predictions of being replaced with some other separation techniques is still the most widely used separation process. The energy inefficiency of the process however, has always been the concern of researchers. This is because of the economic and environmental implications of unutilised energy [1]. The essential need of distillation system coupled with its demanding energy usage has led to a number of methods targeted at improving the effectiveness of the column. One of such methods is through the application of the laws of thermodynamics in the analysis of the column. This has been applied through pinch analysis and exergy analysis [2]. Pinch analysis is a synthesis tool. It shows in which way the heat can be added or extracted and it determines how best to place heating and cooling utilities for optimum energy performance. Pinch analysis is however, limited in its application to systems with heating or cooling requirement [3]. Exergy analysis on the other hand has a wide range of applicability but it is often used as a diagnostic tool to give an indication of how efficient a process is compared to its optimum possible performance [4] and to pinpoint regions of inefficiency in a column [5]. The challenge therefore, is to use exergy in the “how” of making a process efficient.

Diagrammatic representation of the thermodynamic analysis of distillation process has been used by a number of authors to give a better understanding as to what operates within the column. This is with a view to allow the designer or operator to identify useful

modifications that will improve the efficiency and optimization of the column [6]. Dhole and Linhoff [7] considered the column as a reversible column using temperature enthalpy profile in targeting for column modifications. The assumption of reversibility however, limits the application of this method to multicomponent mixtures and though the procedures led to column energy improvement, it does not identify the main sources of irreversibility within the column [8]. An attempt to overcome this deficiency in the thermodynamic analysis of the column led to introduction of the exergy loss profile [9]. Exergy loss profile could describe in a single variable the distribution of multicomponent heat and mass driving forces. It has been previously used in the retrofit of a crude distillation unit [10] and of recent in the optimization of operating parameters such as reflux ratio and feed stage [11]. However, considering the fact that distillation process is hinged on the transfer of mass and heat between two states (liquid and vapour), there is a need for a profile that will diagrammatically show this and as well provide means of improving the column based on the driving forces between the vapour and liquid states.

This present work is set to present exergy rate profiles for the column in atmospheric distillation unit (ADU) of Warri refinery. The exergy rate profiles serve as a tool to pinpoint the source of inefficiencies within the column and as a screening tool to determine retrofit options. The paper also presents exergy rate profiles as having a direct relation with the overall energy consumption of

the column and hence shows a possibility to be used in optimizing the column without violating the specifications of the column. The paper is sectionalised as follows. Section 2 describes the Warri atmospheric distillation unit under consideration. Section 3 gives the exergy analysis and exergy rate profiles concepts while section 4 gives the optimization procedures using Artificial Neural Network. Section 5 presents the results and discussion of the application and section 6 concludes the paper.

2. The System

The schematic diagram of the ADU of Warri Refinery is shown in Fig.1. It operates above atmospheric pressure and is a long column that consists of 46 trays. The atmospheric residue is drawn from the bottom tray. The overhead vapours are condensed in the atmospheric column air cooler and collected in an accumulator. Both column bottom liquid and the liquid side cuts contain light ends. Light ends removal is achieved by injecting steam.

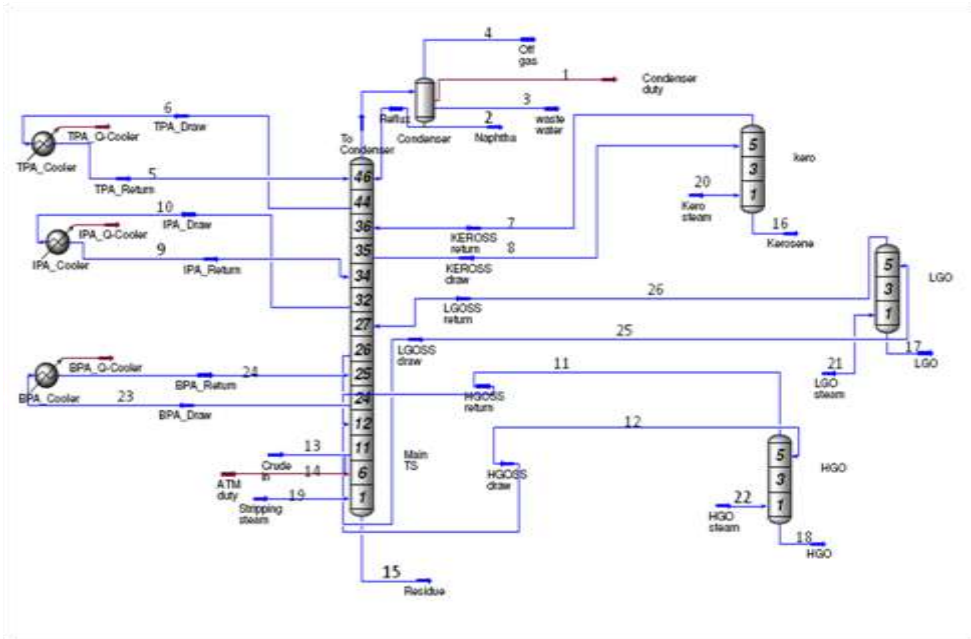


Figure 1: Schematic diagram of the Atmospheric Distillation Unit of Warri Refinery

Three side cuts are drawn respectively from the 35th, 26th and 11th trays and processed separately in the strippers. The kerosene cut is fed into the kerosene stripper above the 5th tray in the stripper, and vapours return to the main column above the 36th tray, while the stripped kerosene is sucked from the bottom of the stripper by a pump and sent to storage. The Light gas oil (LGO) cut is fed into the LGO stripper above

the 5th tray in the stripper, and vapours return to main column above the 27th tray, while the stripped LGO is sent to storage. The heavy gas oil (HGO) cut is fed into the HGO stripper above the 5th tray in the stripper, and vapours return to main column above the 12th tray. The top pump around (TPA), the intermediate pump around (IPA) and the bottom pump around (BPA) are drawn from tray 44, 32 and 24,

respectively before being recycled back to the column after heat exchange.

3. Concepts of exergy and exergy rate profiles

3.1 Exergy analysis

Exergy is a concept from the first and second laws of thermodynamics and its calculation is based on the determination of the enthalpy and entropy of any given system. Usually the physical exergy of a system is calculated as [12]:

$$Ex_{ph} = m((h - h_0) - T_0(s - s_0)) \quad (1)$$

with the reference temperature given as 298K and the reference pressure as 1atmosphere. For chemical processes, the interaction between the chemical species in the system of study and the environmental precursors makes the calculation of the chemical exergy imperative. Different substances have different ways of chemical exergy calculation. For a crude stream which is of high interest here, standard molar chemical exergy is calculated from the standard molar chemical exergies of all identified components and pseudo-component as:

$$\Delta Ex_{ch} = \sum n_i b_{qi} + \sum n_i b_{chi} + RT_0 \sum n_i \ln a_i \quad (2)$$

where b_{chi} is the chemical exergy for component i ; b_{qi} is the chemical exergy for pseudo-component i ; and a_i is the activity coefficient of component i .

The standard chemical exergy for pseudo-components can be determined from heuristic empirical expression as a function of the elementary composition and their heating values [13]. This is calculated as:

$$B_{qi} = \varphi_i C_i \quad (3)$$

where φ_i is the regression equation determined to express the ratio H/C, N/C, O/C and S/C for the pseudo-components (H, C, N, O and S are elements – Hydrogen, Carbon,

Nitrogen, Oxygen and Sulphur); C_i is the net calorific heating value of the pseudo-component i ; and

$$\varphi_i = 1.44H + 0.1773 \frac{H^2}{C} + 0.1431 \frac{H^3}{C} + 0.2089 \quad (4)$$

where z is compressibility factor. Total exergy of a stream is then calculated from the addition of the physical and chemical exergy of the stream.

Exergy losses in thermal process could be internal loss as a result of irreversible phenomena in the process plant or external loss as a result of waste products from the process. Major losses in the column are considered to be from internal losses. Hence the overall exergetic efficiency of the column is defined as:

$$\eta = \frac{\text{Exergy of useful products}}{\text{Exergy of feed}} \quad (5)$$

For the ADU, the exergetic efficiency was defined as:

$$\eta = \frac{\sum_{i=1}^n \dot{Ex}_{out,i}}{\sum_{i=1}^n \dot{Ex}_{in,i}} = \frac{\dot{Ex}_{x26} + \dot{Ex}_{x17} + \dot{Ex}_{x18} + \dot{Ex}_{x19} + \dot{Ex}_{x20} + \dot{Ex}_{x21} + \dot{Ex}_{x22}}{\dot{Ex}_{x12} + \dot{Ex}_{x13} + \dot{Ex}_{x14} + \dot{Ex}_{x15} + \dot{Ex}_{x16} + \dot{Ex}_{x17} + \dot{Ex}_{x18} + \dot{Ex}_{x19} + \dot{Ex}_{x20} + \dot{Ex}_{x21} + \dot{Ex}_{x22}} \quad (6)$$

The exergetic efficiency of the side strippers were also calculated as:

$$\eta_{s1} = \frac{Ex_{x26} + Ex_{x17}}{Ex_{x25} + Ex_{x21}} \quad (7)$$

$$\eta_{s2} = \frac{Ex_{x11} + Ex_{x18}}{Ex_{x12} + Ex_{x22}} \quad (8)$$

$$\eta_{s3} = \frac{Ex_{x7} + Ex_{x16}}{Ex_{x8} + Ex_{x20}} \quad (9)$$

where η_{s1} , η_{s2} , and η_{s3} are efficiencies for LGO, HGO and Kerosene side strippers. The numbers are representing the streams as given in Figure 1. Irreversibility, I , was also calculated as:

$$I = \sum Ex_{in} - \sum Ex_{out} \quad (10)$$

3.2 Exergy rate profiles

The calculation of exergy rates for each stage in the liquid and vapour states for binary distillation system has been reported earlier [14, 15] and is now being applied to multicomponent

distillation system. It is calculated for the liquid and vapour states of each tray as:

$$\Delta Ex_{tray} = \Delta H - T_0 \Delta S \quad (11)$$

$$Ex_{iL} = (h_{iL} - h_{0iL}) - T_0 (s_{iL} - s_{0iL}) \quad (12)$$

where Ex_{iL} is exergy of liquid stream of tray i ; h_{iL} is enthalpy of liquid stream of tray i ; F_{iL} is liquid flow rate of tray i ; h_{0iL} is enthalpy of liquid stream of tray i at reference conditions; T_0 is the reference temperature = 298.15 K; s_{0iL} is the entropy of liquid stream of tray i at reference conditions; and s_{iL} is the entropy of liquid stream for tray i , and is given by the equation 13:

$$s_{iL} = h_{iL} \frac{\left(\ln \frac{T_i}{T_0} - R \ln \frac{P_i}{P_0} \right)}{T_i - T_0} \quad (13)$$

where T_i = Temperature of tray i ;
 P_i = Pressure of tray i ; R = Gas constant = 8.314kJ/kmolK; P_0 = 101.3kPa.

Similarly, the vapour stream equations are:

$$Ex_{iV} = (h_{iV} - h_{0iV}) - T_0 (s_{iV} - s_{0iV}) = \Delta H_{iV} - T_0 \Delta S_{iV} \quad (14)$$

$$s_{iV} = h_{iV} \frac{\left(\ln \frac{T_i}{T_0} - R \ln \frac{P_i}{P_0} \right)}{T_i - T_0} \quad (15)$$

Exergy rate profiles are therefore a plot of tray number versus exergy of

liquid state (Ex_{iL}) and exergy of vapour state (Ex_{iV}).

4. Optimization procedures using Artificial Neural Network

4.1 Model Formulation

The model building process was done in four sequential steps, namely: Data processing, Network creating, Network training and testing, and Analysis of the network performance. Neural network training can be made more efficient when certain preprocessing steps are performed on the network inputs and targets. Network-input processing functions transform inputs into a better form for the network use. Post-processing steps transform outputs back to the characteristics of the original target data. The function “Mapminmax” was used to scale the inputs and targets so that they always fall within a specified range before training began. The “Newff” network function which creates a feed forward back propagation network was used. “Trainlm” is the network training function that was used. The networks were trained using supervised learning algorithm. The Levenberg-Marquardt back-propagation learning algorithm was used. The algorithm divides the data into three partitions, namely: the training data set, the test data set and validation data set. 80% of the data was used for the training data, 10% for the testing and the remaining 10% for the validation. The training data set is for the training purposes; the test data is to check the generalization performance of the trained neural network model. The training was stopped when the performance on the test data set results into minimum model error. The validation data set is to validate the model. The performance function used was the mean square estimate (MSE). It

measures the network performance according to the mean of squared errors given in equation (16).

$$MSE = \frac{1}{Q} \sum_{k=1}^Q [T_i(k) - a(k)]^2 \quad (16)$$

A flow chart depicting the processes involved in the modelling is shown in Figure 2.

4.2. Genetic algorithm optimization

The genetic algorithm is a method for solving both constrained and unconstrained optimization problems that is based on natural selection, the process that drives biological evolution. The genetic algorithm repeatedly modifies a population of individual solutions. At each step, the genetic algorithm selects individuals at random

from the current population to be parents and uses them to produce the children for the next generation. Over successive generations, the population "evolves" toward an optimal solution. The genetic algorithm (GA) uses three main types of rules at each step to create the next generation from the current population:

- i. Selection rules select the individuals, called parents that contribute to the population at the next generation.
- ii. Crossover rules combine two parents to form children for the next generation.
- iii. Mutation rules apply random changes to individual parents to form children.

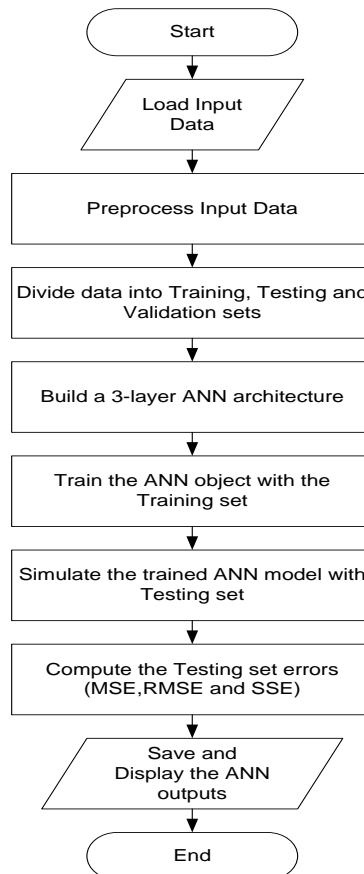


Figure 2: Simulation flow chart of the neural network

The GA optimization problem of the ADU can be stated as:

$$\text{Max } f(x, m, y) \quad (17)$$

$$x_a \leq x \leq x_b$$

$$y = U(x, m)$$

where f is the objective function; x is the controllable variables; m is the uncontrollable variables; y is the efficiency of the column; U is the knowledge database (neural network model) of the crude distillation system; and the notation of a and b represent the lower bound and the upper bound, respectively.

5. Results and Discussion

5.1 Exergy analysis

Table 1 shows the state parameters for the refinery simulation and the material streams that were considered in the analysis. The results of the analysis for the refinery are given in Table 2. The physical exergy efficiency of the ADU is 33.27% with an irreversibility of 4.2×10^8 kJ/h while the total exergy efficiency (physical + chemical) is 33.34%. Here the contribution of the chemical exergy to the efficiency is insignificantly low (0.07%). The low value might result from the lack of chemical reaction taking place in the column. The distillation process is basically a physical operation resulting

from the differences in boiling points of components in the process. A reactive distillation process will have a higher level of contribution from chemical exergy.

The low efficiency of the ADU is suggesting a serious need for improvement of the column for better energy utilisation. The operation of a distillation unit involves the use of a high exergy content steam that is ejected in a low temperature condenser. The area of concentration for the improvement of the process will therefore be on the column. This is attested to from the efficiencies of the side strippers as listed in Table 2. The efficiencies in percentages are 93.93, 94.40 and 87.52 for KERO, LGO and HGO side strippers, respectively.

The energy efficiency of the ADU is 86.48%. This is far apart from the exergy efficiency result. It has been confirmed that efficiency of processes is better analysed using the second law of thermodynamics rather than the first law. The overall exergy efficiency of the unit (ADU+Prelash) is 3.64%. The contribution of ADU to this inefficiency is greater and much work should be concentrated on the ADU for the overall improvement of the unit.

Table 1: Material streams parameters from the simulation of the Atmospheric Distillation Unit

Stream No	Stream Name	Temperature (°C)	Pressure (kPa)	Molar Flow (kgmol/h)
2	Naphtha	184.3	45	3387
3	Waste water	184.3	45	0.0000
4	Off gas	184.3	45	7106
5	TPA return	164	50.2	8284
6	TPA draw	232	50.2	8284

7	KEROSS draw	258	70.48	164.2
8	KEROSS return	264.1	70.48	2090
9	IPA return	207.1	77.4	1.373e4
10	IPA draw	275.1	77.4	1.373e4
11	HGOSS return	323.5	124.6	90.90
12	HGOSS draw	332.5	124.6	518.4
13	Crude in	350	156.9	1.914e4
15	Residue	324.8	147.1	3455
16	Kerosene	243.6	70.48	1962
17	LGO	277.3	90.76	3123
18	HGO	296.5	103.4	455.7
19	Stripping steam	151.8	500	95130
20	Kero steam	151.8	186.3	36.08
21	LGO steam	151.8	205.9	83.26
22	HGO steam	151.8	225.6	27.75
23	BPA draw	308.4	95.27	6233
24	BPA return	278.5	95.27	6233
25	LGO draw	300.7	90.76	3378
26	LGO return	293.8	90.76	3378

Table 2: Efficiency Calculations for ADU base case

	Exergy Efficiency (%)	Energy Efficiency (%)	Irreversibility (kJ/h)
ADU	33.27	86.48	4.179×10^8
LGO	94.40	≈ 100	2.56×10^6
HGO	87.52	≈ 100	1.149×10^6
KERO	93.93	≈ 100	1.18×10^6

5.2 Exergy Rate Profiles

Distillation process is hinged on the principle of heat and mass transfer between the liquid and the vapour state on a stage by stage level. The in-depth study of states' interaction on each stage is therefore necessary. The exergy rate profile simultaneously describes the first and second laws of thermodynamics on a single diagram and hence gives a better insight between the liquid and the vapour state. The exergy rate profiles show the distribution of driving forces within the column between the liquid and the vapour states of each tray. The profiles equally show the feasibility of the column design. A crossing of the profiles is thermodynamically infeasible and connotes an infeasible design [14, 15].

In Figure 3, a crossing of the profiles is noticed showing that there are points within the column when the exergetic liquid phase flow is higher than the vapour flow and creating pinch points that are contributing to the inefficient performance of the column. Exergy rate profiles are calculated putting temperature and mass flow of the phases under consideration; there are no temperature and mass transfer driving

forces at these points of crossing. These are indicators of sources of inefficiency within the column. Exergy rate profiles can be used for targeting possible ways of column modifications right at the design stage.

Usually, ways of reducing dissipated energy in processes is to increase the process reversibility by increasing equipment size. A better way however will be to localise the energy supplied within the process by distributing the driving force evenly and exergy rate profile will give an indication of whether this has been achieved and hence, instilling confidence for an efficient design or stimulating the designer for a better column performance.

A marked difference is noticed on the sixth stage. This stage is the feed stage of the refinery. This is indicating some other factors that are contributing to the inefficiency of the column. The feed conditions of the refinery might not be adequate. The inappropriate feed condition causes a sharp change in the exergy rate profiles near the feed stage. This is in line with the work of Dhole and Linnhoff [7] on the use of column grand composite curve (CGCC) for column modifications. The sharp rise in

the vapour profile suggests an excessive heat supply for the feed stage and ultimately an unnecessary condenser load. Exergy rate profiles make it easy to see a feed which is excessively heated or subcooled and hence, minimises the condenser and reboiler load. However, because of the fact that there is a limit at which the inlet temperature of the crude can be raised to prevent cracking [16] and considering the reality that the ratio of the crude to the stripping steam is less than that suggested in the literature (5-10%), the line of increasing steam flow rate may be considered. The exergy rate profiles also show modification for side condensing/reboiling of the column. The kinked nature of the liquid phase curves occurred in the column at the tray where pump around flow are

returned to the column. This kinked nature is suggesting modifications for the pump around flow for an efficient design.

Attempts were made to remove the crossing of the profiles by altering the feed condition and the stripping steam flow rate. The result is given in Figure 4. If the kinked nature of the profiles is removed and there is a reduction in the driving force, it will give a much higher efficiency. Another way is to consider optimizing the column operating conditions for the optimum combinations of the operating parameters that will result in exergy rate profiles not crossing each other with the column efficiency being the objective function. This was explored next using expert system.

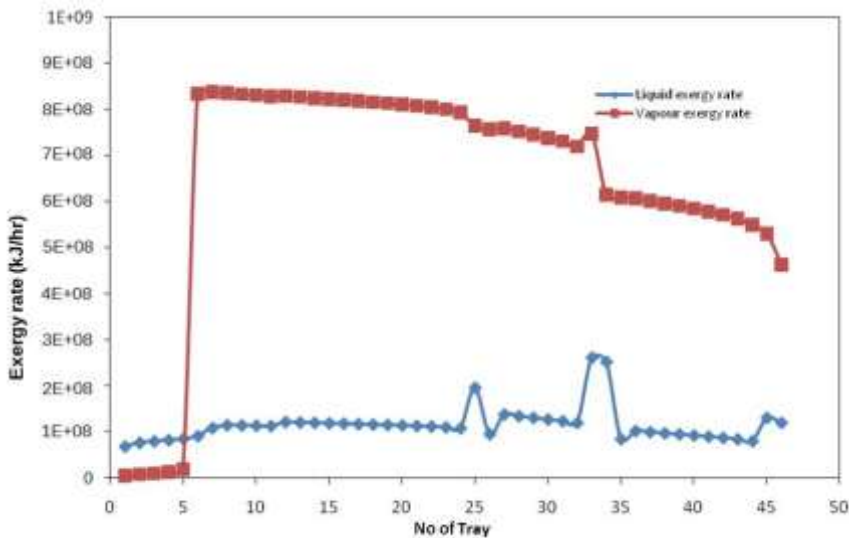


Figure 3: Exergy rate profile for Warri ADU base case

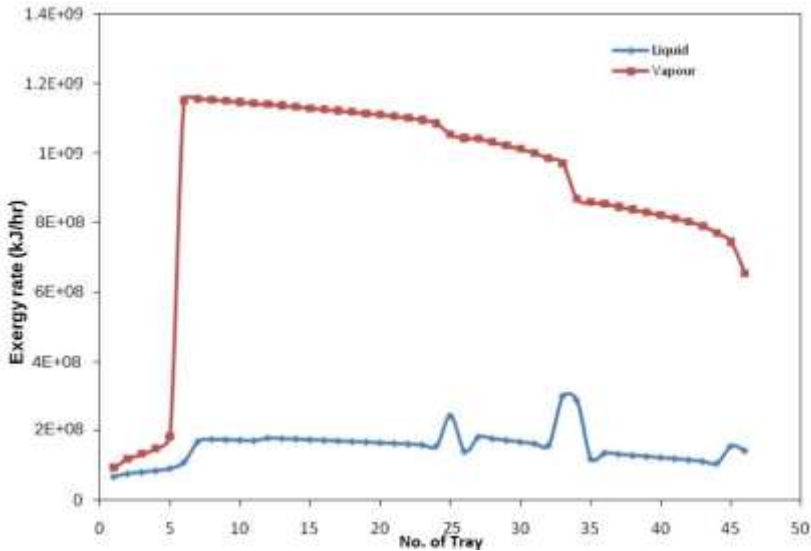


Figure 4: Exergy rate profile for Warri ADU (Crossing removed)

5.3 Neural Network Model

The NN model was trained to represent the knowledge data base of the ADU operating system using the ADU simulated runs from HYSYS. Two thousand and thirty four (2034) data sets were used in training the ADU for the refinery. 10% of the data set was used to test the trained model. The result of comparison between the real/actual data output and the target output from the model shows that the models predict the actual data accurately. Liao et al. [17] and Motlaghi et al. [18] obtained similar result though their data were basically experimental.

The correlation coefficient of the ANN model was 0.9999. This implies that the relative error of the trained model and the tested data was below 1×10^{-4} , showing that the NN model was quite reliable in describing the input-output relationship of the ADU. The NN model was able to adequately represent

the complex process of the ADU due to the non-linear characteristics of the NN structure. Figure 5 also illustrate the best linear regression fit of the output and the target data of the refineries which in each case approaches 1. The validation performance parameter is 0.0010531. All these are good indicators that the trained models for the refineries predict accurately. The models therefore can be used to determine the outcome of changes in any of the given input parameters; it can correlate the relationship between the input and output variables of the refinery. It can also predict and point out the effects of the operating variables on the products of the refinery as well as the efficiency of the ADU. This will either serve as stimuli to operators that the operating conditions are ideal for an efficient column or as impetus that better combinations of operating conditions can be searched for.

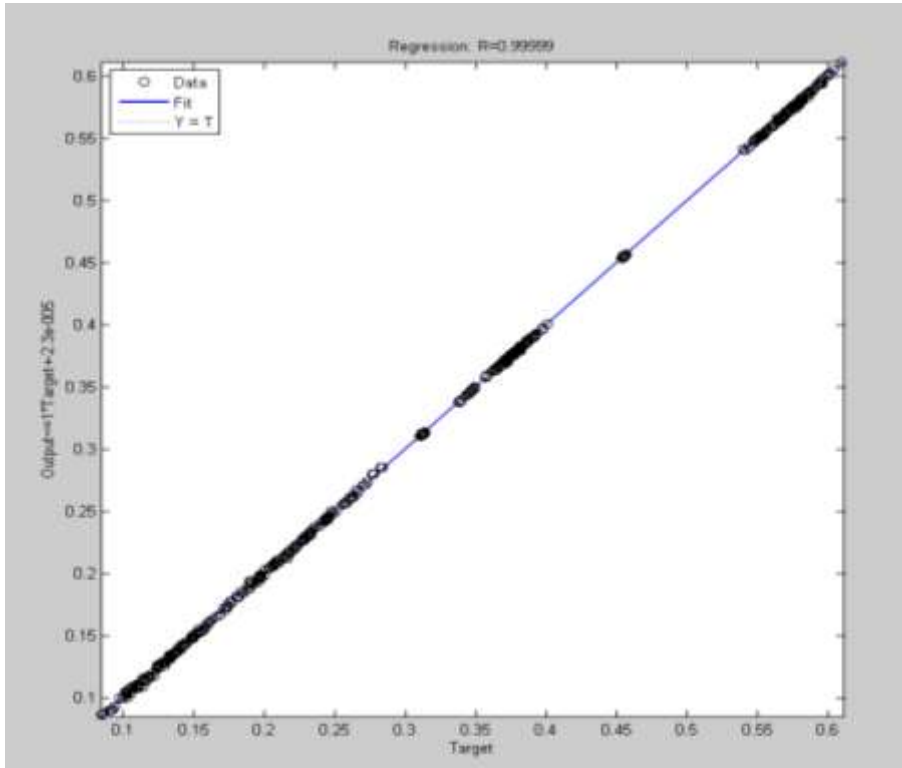


Figure 5: Correlation between the NN predicted values and simulated

5.4 Genetic algorithm optimization

The genetic optimization was done for the existing operating conditions of the refineries and the operating conditions resulting from the exergy rate profile. The optimization problems here consist of an objective function to be maximised together with constraints from design and operation conditions. The objective function is the exergy efficiency, subject to the constraints of the given controllable variables with the following upper and lower boundaries:

$$300 \leq \text{Feed temperature} \leq 360$$

$$3e4 \leq \text{Steam mass flow} \leq 1e5$$

$$220 \leq \text{Steam temperature} \leq 260$$

$$5434 \leq \text{TPA rate} \leq 1.09e5$$

$$2.1e4 \leq \text{IPA rate} \leq 5.43e4$$

$$1.63e4 \leq \text{BPA rate} \leq 1.41e5$$

$$86.4 \leq \text{TPA}\Delta T \leq 176.4$$

$$68.4 \leq \text{IPA}\Delta T \leq 158.4$$

$$86.4 \leq \text{BPA}\Delta T \leq 176.4$$

Thus a total of nine process variables were used for the optimization. The knowledge database of the neural network model was used in the optimization procedures. About 100 generations were made and the output with the least error was returned as optimum. The corresponding efficiency for these combinations was 53%. This is a great improvement from an initial efficiency of 33%. The optimum input from the optimization procedures were also validated in HYSYS and the efficiency was close to that predicted. The expert system can be said to adequately predict the optimum conditions at which the ADU can operate with the least irreversibility. The operating conditions that led to the removal of the crossing were also

optimised and a new set of optimum conditions that give a non-crossing exergy rate profiles were found. The efficiency at this point was 60% showing a marked increase of 7% to the optimum efficiency when the exergy rate profiles were not considered. The exergy rate profile which gives feasible thermodynamic conditions of the column also gives a higher thermodynamic efficiency and hence it's a preferred method of column optimization. Table 3 gives the base case operating conditions, the optimum operating conditions for the base case

and the optimum operating conditions for the exergy rate profiles (ERP) modified case.

6. Conclusion

Artificial neural network method of optimization afforded the means of using up to nine operating variables in optimizing the operation of an atmospheric distillation unit in a crude distillation unit of a refinery which resulted in a 20% increase in exergy efficiency. Exergy rate profiles were calculated putting temperature and mass flow rates of the

Table 3: Comparison between base case, optimum values of the base case and ERP modified case

	Base case	Optimum base case	Optimum ERP modified
Feed temperature $^{\circ}\text{C}$	350	300	307
Steam flow Kg/h	5285	4183	7226.4
Steam Temperature	151.8	231	232
TPA rate barrel/day	1250	7747	6164
IPA rate barrel/day	2072	85044	21807
BPA rate barrel/day	9409	38640	84424
TPA ΔT $^{\circ}\text{F}$	154	109	92
IPA ΔT $^{\circ}\text{F}$	154	79	73
BPA ΔT $^{\circ}\text{F}$	86	134	131
Efficiency %	33	53	60

phases into consideration. When the profiles cross each other there are no temperature and mass transfer driving forces at these points of crossing. These are indicators of sources of inefficiency within the column. The exergy rate profiles revealed the source of

inefficiency within the column. It was used to target possible ways of column modifications. The crossing of the profiles was removed and it further improved the exergy efficiency of the column by 7%.

References

1. M.A. Rosen and I. Dincer, "On exergy and environmental impact," *International Journal of Energy Research*, 21(7), pp. 643-654, 1997.
2. Y. Demirel, "Thermodynamic analysis of separation system," *Separation Science and Technology*, 39, pp. 3897-3942, 2004.
3. M.A. Gadalla, O.Y. Abdelaziz and F.H. Ashour, "Conceptual insights to debottleneck the network pinch in heat integrated crude oil distillation systems without topology modifications", *Energy Conversion and Management*, Volume 126, pp 329-341, 2016
4. A. Doldersum, "Exergy analysis proves viability of process modifications," *Energy Conversion and Management*, 39(16-18), pp. 1781-1789, 1998.
5. S.F. Wang, T. Ma, G. Gao, P. Wu and L. Liu, "Energy and exergy analysis of a five-column methanol distillation scheme." *Energy*, Volume 45, Issue 1, pp. 696-703, 2012.
6. R.J. Zemp, S.H.B. de Faria and M.d.L. Oliveira Maia, "Driving force distribution and exergy loss in the thermodynamic analysis of distillation columns," *Computers & Chemical Engineering*, 21, Supplement, pp. S523-S528, 1997.
7. V.R. Dhole and B. Linnhoff, "Distillation column targets," *Computers & Chemical Engineering*, 17(5-6), pp. 549-560, 1993.
8. R. Smith and R.J. Zemp, (eds.) *Process integration of separation systems* Rugby, UK: IChemE. 1994.
9. S.H.B. Faria and R.J. Zemp, "Using exergy loss profiles and enthalpy-temperature profiles for the evaluation of thermodynamic efficiency in distillation columns," *Thermal Engineering*, 4, pp. 76-82, 2005.
10. A.H. Tarighaleslami, M.R. Omidkhan, A. Ghannadzadeh and R.H. Hesas, "Thermodynamic evaluation of distillation columns using exergy loss profiles: a case study on the crude oil atmospheric distillation column," *Clean Technologies and Environmental Policy*, 14(3), pp. 381-387, 2012.
11. L.B. Rocha, M.L. Gimenes, S. Farai, L. Jimenez and T. Cavali, "A new methodology to reduce exergy loss of distillation columns using rigorous process simulation," *Computer Aided Chemical Engineering*, Volume 38, pp. 1003-1008, 2016.
12. J. Szargut, D.R. Morris and F.R. Steward, *Exergy analysis of thermal, chemical and metallurgical processes*. New

- York: Hemisphere Publishing Corporation, 1998.
13. R. Rivero, C. Rendon and L. Monroy, "The Exergy of Crude Oil Mixtures and Petroleum Fractions: Calculation and Application," *International Journal of Thermodynamics*, 2(3), pp. 115-123, 1999.
 14. A.N. Anozie, A.S. Osunleke and T.C. Aseeperi, "Exergy analysis and optimisation of binary plate distillation column operations," *International Journal of Exergy*, 7, pp. 593-606, 2010.
 15. A.N. Anozie, F.N. Osulale and A.S. Osunleke, "Exergy analysis of binary plate distillation column operations," *International Journal of Exergy*, 6, pp. 715-728, 2009.
 16. J.H. Gary and G.E. Handwerk, *Petroleum refining*. Taylor and Francis, 2001.
 17. S. Motlaghi, F. Jalali and M.N. Ahmadabadi, "An expert system design for a crude oil distillation column with the neural networks model and the process optimization using genetic algorithm framework," *Expert systems with applications*, volume 35(4), 1540-1545, 2008.
 18. L.C. Liau, T.C. Yang, and M. Tsai, "Expert system of a crude oil distillation unit for process optimization using neural networks," *Expert systems with applications*, volume 26(2), 247-255, 2004.



Assessment of Pre-Stressed Concrete Electric Poles for Rural Electrification Projects

Adegboyega G. A.¹ & Adewuyi P. A.²

¹Covenant University, Canaan Land, Ota, Nigeria

²Bells University of Technology, Ota, Nigeria

¹gabrieladis@yahoo.com;

²solaadewuyi@gmail.com

Abstract: Rural electrification is the process of bringing electrical power to rural and remote areas in a country in order to improve the living conditions of the people. In accordance with the extant electricity regulation act chapter 106 Laws of the Federal Republic of Nigeria (1990) Part VI No 47 (i), every support carrying electric lines shall be made of treated wood, steel or reinforced concrete or any combination of such materials or other approved materials. Regulation No 47, (2)(1990), further stipulates that every support shall be so constructed to withstand the transverse, horizontal and vertical loads. Hence, in order to confirm that any pre-stressed concrete electric pole is acceptable and fit with adequate strength for rural electrification projects, a test or assessment was carried out. After the test, a safety factor of above 2.0 units was obtained and the cube test result satisfied the minimum strength of 40N/mm² for the pre-stressed concrete pole.

Keywords: Pre-stressed concrete electric poles, factor of safety, tensile strength, concrete cube, concrete mix, rural electrification.

1. Introduction

Electricity plays a very important role in the socio-economic and technological development of every

nation. Significantly, rural electrification is the backbone of rural economy and basic input for rapid rural development. Rural electrification is

the process of bringing electrical power to rural and remote areas in a country in order to improve the living conditions of the people. As a result of this gesture, electricity would be available for lighting and household purposes and would also assist in agriculture mechanization practice. Hence, rural electrification is the main infrastructure for ensuring speedy growth of the agricultural sector and agro-based industrial structure in rural areas.

Furthermore, in order to control population drift from rural areas to urban areas, the Nigerian Federal Government set up Rural Electrification Agency (REA) with statutory function to electrify the rural areas and the border towns in the country.

The Rural Electrification Programme was initiated in 1981 by the Federal Ministry of Power and Steel. A major strategy of the programme was to extend electricity to all 774 local government headquarters in the country and border towns. The Rural Electrification Agency is established to carry out the following functions:

- i. Promote rural electrification in the country;
- ii. Co-ordinate federal and state rural electrification activities; and
- iii. Establish and manage the Rural Electrification Fund (REF).

The objectives of Rural Electrification are to: (a) promote agriculture, industrial, commercial, economic and social activities in rural areas through provision of good quality and affordable electricity; and (b) raise the living standards of the rural population through provision of adequate pipe borne water supply, available uninterrupted electricity supply and ensure adequate security for the

populace, in order to assist in reducing rural-urban migration.

2. Rural Electrification Distribution System

The distribution system is one of the three components of an electric power system, that is, generation, transmission and distribution. Ewesor (2010) expressed the fact that the distribution involves primary and secondary transformation of high voltage to the standard medium of low voltage by the appropriate transforming equipment. A distribution network connects all loads in a particular area to the transmission line or network. The distribution network design, planning and operations are of great importance in the quest towards the provision of continuous stable electric power. Desphande (2006) states that the network distribution system is applicable in large loads and where the system has to be made more reliable for continuity of power supply. He stated further that to start designing the rural distribution system, the first requirement is to predict or know the load in the area.

According to Pabla (2008), the distribution system is part of the system between transmission and the consumer service point.

It contains:

- (i) Sub-transmission circuits in voltage ratings usually between 33kV and 220kV which deliver energy to distribution substation;
- (ii) Primary circuits of feeders operating in the range of 11kV to 33kV and supplying the load in a well-defined geographical area; and
- (iii) Distribution transformer are installed on poles or on plinth or near the consumer's sites which transforms

the primary voltage to secondary voltage usually 240/415V.

In addition, Garg and Uppal (2011) expressed the fact that all the equipment in the distribution substation, overhead lines, and underground cable radiating from the distribution substation combined together are known as distribution system.

The empirical formula (Gupta, 1998) for calculating the optimum voltage of primary distribution system is given as:

$$V_L = 5.5 \sqrt{\frac{L}{1.6} + \frac{P_L}{100}} \dots \dots \dots (1)$$

where VL is the line voltage in kV, L is the length of the line in km and PL is the power in kW.

According to popular saying by cable manufacturers, "Electricity has no legs but has to be carried by conductors". Conductors carry electric power from the sending-end station to the receiving-end station. The common conductors used for overhead lines are copper, aluminium, steel-cored aluminium, galvanized steel and cadmium copper. In this country, aluminium conductors are used for low voltage distribution lines with varying sizes from 35mm², 50mm², 70mm², 100mm² and 150mm².

For 11- kV and 33-kV distributions, the conductor used is the steel-cored aluminium, and it is also known as aluminium conductor steel reinforced (ACSR) of various sizes of 70mm², 100mm² and 150mm².

Electricity is carried by wires supported by reinforced concrete poles. These poles have become very popular as line supports for township distribution and for rural electrification schemes. They have greater mechanical strength, longer life span, and permit longer spans than wooden poles. They give good outlook and require little

maintenance. They have good insulating properties. The holes in these poles facilitate climbing of the poles and at the same time reduce the weight of the line supports.

The overhead power line is designed by keeping in view the electrical and mechanical requirements. Wind pressure on poles and conductors are calculated as per the basic wind speeds given in International Standard: 802 (Part I, Section 1 of 1995). This is given as

$$P = 0.6V_d^2 \dots \dots \dots (2)$$

where P is design wind pressure in N/m² and Vd is design wind speed in m/s.

During the construction of rural electrification line, it was observed that when 100-mm² aluminium conductor steel reinforced (ACSR) is shrunk on cross-arms supported by reinforced concrete poles, these poles got cut-off from the top thus making them useless. The cutting off action of the poles results in delay in rural electrification projects due to cutting corners by the electrical contractors. Hence, investigation and test were carried out on reinforced concrete poles used for rural electrification projects.

The rural electrification scheme demands careful supervision, monitoring, valuation and testing to ensure that the requirements and specifications for quality assurance are strictly adhered to during construction stage.

3. Reinforced Concrete Pole Production and Testing

According to Chandra and Gehlot (2004), cement is a cementitious material which has the adhesive and cohesive properties necessary to bond inert aggregates into a solid mass of adequate strength and durability.

Cement is the most important constituent of concrete.

Chandra and Gehlot (2004) stated further that a carefully proportioned mixture of cement (used as binder), fine aggregate (sand), coarse aggregate (gravel) and water. This mixture which hardens to a stone-like mass, is called concrete. They emphasized that the steel bars are used to reinforce the concrete. The steel bars which are completely surrounded by hardened concrete form internal part of the structural member. Hence, in such a manner, the steel bars and concrete act together in resisting forces. The concrete reinforced with the steel bars is known as reinforced concrete.

The pole is designed for bending strength. If W denotes the load in kg applied at 0.30m from the top of pole, then; we have

$$M = fz \dots\dots\dots(3)$$

where M is sum of the bending moments of the loads on the pole at ground level, z is modulus of the section of pole; and f is the fibre stress maximum.

Concrete poles of ratio 1:1.5:3 with 15mm size well-graded shingle are used for construction of the lines.

Casting of the poles is carried out by arranging a network of 8mm² high tensile reinforcement steel wires in moulds with the help of 6mm² link, pouring in a well-mixed concrete into the mould to cover the arranged reinforcing iron rods. The moulded reinforced pole would be fabricated by compacting the concrete with vibrators. The resulting moulded reinforced poles would then be placed into the curing bath (tank) which is full of water.

The poles are normally left in the bath (tank) for 5 to 12 days, after which they are taken out of the bath (tank) and

subjected to another 4 to 16 days of wetting with water by sprinkler in the open air after which they are ready for use.

The re-inforcement of the 10.40-m pole is produced in the factory with 8 in number reinforcing irons embedded in it while the reinforcement of the 8.5-m pole is produced in the factory with 6 in numbers reinforcing iron rods embedded into it.

The tensile strength and Young modulus of elasticity of the reinforcement rods were determined by Avery Testing Machine. The tensile strength of iron rods was above 160kg/cm².

The poles that have been cured for more than 21 days were tested. The reinforced concrete poles were fixed horizontally and were rigidly supported up to a length of about 1.46m for 8.5m pole from the butt end. The load was applied at right angles to the axis of the pole at a point 0.6m from the top end of the pole. The free part of the pole was laid on smooth surfaced wooden planks to reduce the induced bending moment due to the weight of the pole. The applied loads were read on a dynamometer scale. The pole was subjected to the following types of test:

(a) The elastic phase test: the appropriate loads in graduated steps of 0%, 20%, 40%, 60%, 80% and 100% of the working load were applied. The deflection was measured at the point of application of the load; the numbers and locations of hair cracks were noted. The load was then reduced to zero and the deflection at that instance was noted.

(b) The breaking phase test: the loading was graduated in steps until the pole was destroyed. The hair cracks and deflection at each loading step and the

length from the butt to the breaking point were noted.

Table 1: Pole Types under Test

Parameter	Pole A	Pole B
Pole length (m)	10.40	8.5
Weight (kg)	900	700
Butt dimension (mm)	250 x 380	240 x 350
Top dimension (mm)	150 x 150	150 x 150
Number of reinforcing iron rods	8	6
Rigid support from butt end (m)	1.96	1.46
Point of load application from top (m)	0.6	0.6
Working load (kg)	300	240

4. Results and Discussion

The test results for type A pole is shown in table 2 while that of type B pole is shown in table 3.

Table 2: Pole Type A Test Result

Percentage Loading (%)	Applied Load (kg)
0	0
20	60
40	120
60	180
100	240
110	300
120	360
140	420
160	480
180	540
200	600
220	660
240	680

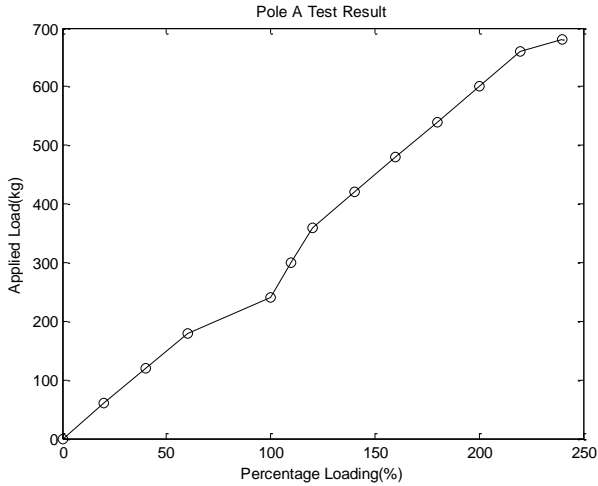


Figure 1: Pole ‘A’ Test Result

The pole broke when applying the last load of 680kg at 1.6m from the butt end. By definition,

$$safety\ factor = \frac{ultimate\ load}{working\ load} = \frac{680}{300} = 2.3.....(4)$$

Table 3: Type B Pole Test Result

Percentage Load (%)	Applied Load (kg)	Deflection (mm)
0	0	0
20	48	0
40	96	2.5
60	144	2.5
80	192	6.7
100	240	12.8
120	288	18
140	336	27
160	384	35
180	432	110
200	480	Pole broke

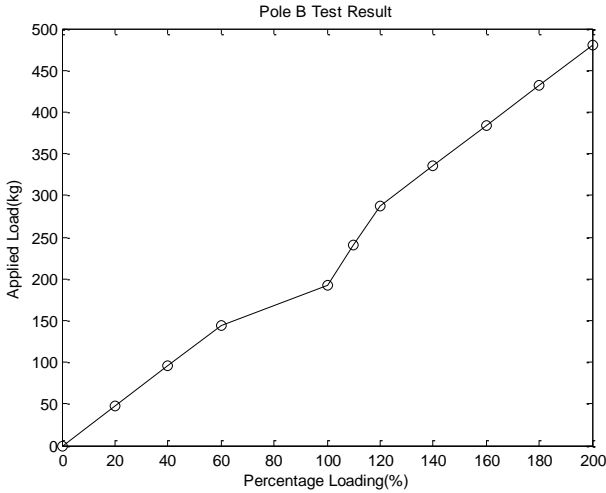


Figure 2: Pole 'B' Test Result

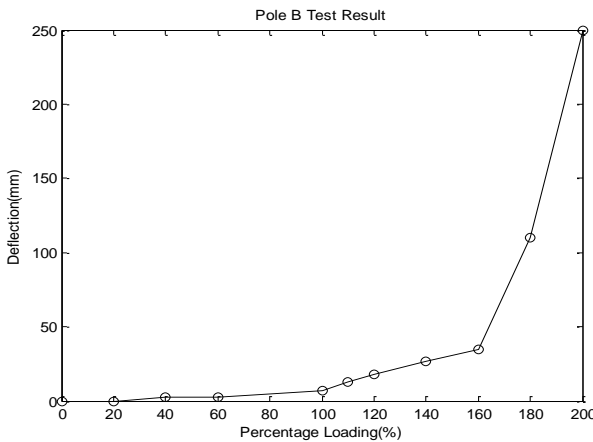


Figure 3: Pole 'B' Test Result for Deflection

The pole broke when applying the load of 480kg at 1.7m from the butt end.

By definition

$$safety\ factor = \frac{ultimate\ load}{working\ load} = \frac{480}{240} = 2.0$$

.....(5)

Variation in the number of iron rods used for reinforcement could give rise to varying tensile strength of the concrete poles. From the graph of fig. 1 and the result of the tested concrete poles and the observation made from the broken poles, it could be concluded that the broken poles were not

constructed according to the standard specifications due to sub-standard materials which resulted in structural failure.

Conclusion

- (i) The straight through reinforcement iron rods should not be jointed en-route to prevent breaking of the poles at the point of joints.
- (ii) The reinforcement network for moulds should not be reduced under the disguise of economics in material use.

- (iii) The poles manufacturing procedure should be subjected to occasional random test and inspection.
- (iv) All poles should incorporate built-in earthing wire to enable overhead earthing points to be connected to earth rods at the base of the pole.
- (v) Concrete electric poles should be purchased by electrical contractors from government approved manufacturers, hence concrete

reinforced electric poles that satisfied the conditions stipulated by Electricity Supply Regulation 133 of chapter 57 of the Laws of the Federal Republic of Nigeria, Part VI No 53 Electricity Act CAP 106 Laws of the Federal Republic of Nigeria (1990) and the relevant British Standard and International Standards should be used for Rural Electrification Projects.

References

- Chandra Ram and Gehlot Virendra (2004) Elements of Limit State Design of Concrete Structures, Scientific Publishers, India.
- Desphande M. V. (2006) Electrical Power System Design (26th Edition), Tata McGraw-Hill Publishing Company Limited, New Delhi, India.
- Ewesor P. O. (2010) Practical Electrical Systems Installation Work and Practice (2nd Edition), Petvirgin Patrnrs, Benin City, Nigeria.

- Gupta B. R. (1998) Power System Analysis and Design, S. Chand and Company Ltd., New Delhi, India, pp. 209-228, 503.
- Laws of the Federal Republic of Nigeria, Chapter 106 of 1990 – Electricity Regulations.
- Pabla A. S. (2008) Electric Power Distribution (5th Edition), Tata McGraw-Hill Publishing Company Limited, New Delhi, India.



Comparative Study of the use of Arithmetic Mean and Geometric Mean for Data Aggregation in FMEA Analysis

¹Ikuobase Emovon & ²Modestus Okechukwu Okwu

^{1,2}Department of Mechanical Engineering,
Federal University of Petroleum Resources, Effurun, Nigeria

Abstract: Failure Mode and Effects Analysis (FMEA) is a commonly use approach for ranking risk of failure modes of most marine machinery system. However, the Risk Priority Number (RPN) use for evaluating risk within FMEA framework have several limitations and as such most researchers focus had been in the area of improvement of the tool without considering the effect of the aggregated data from multiple experts use as input into the decision making process. The purpose of this paper therefore, is to perform a comparative analysis of the aggregation techniques for combining multiple experts' ratings of failure modes in order to establish their degree of similarity and their effect on the output of the ranking tools. The commonly used aggregation techniques in the literature considered are; Arithmetic Mean (AM) and Geometric Mean (GM). The index for comparison of the AM and GM was based on the effect of their respective aggregated data on the rank produced by four well known ranking tools; RPN of FMEA, Compromise Programming (CP), Vlsekriterijumska Optimizacija Ikompromisno Resenje, meaning: Multicriteria Optimization and Compromise Solution (VIKOR), Weighted Sum Model (WSM) and Weighted Product Model (WPM). A case study of fuel oil system of marine

diesel engine of ship system was utilised to demonstrate the effectiveness of the two techniques.

Keyword: Arithmetic Mean, Geometric Mean, Failure modes, Aggregation techniques, MCDM, FMEA

1. Introduction

One of the major element of any maintenance system is risk assessment, this is because generally the maintenance strategy that need to be implemented for plant system maintenance will depend on it degree of risk. Failure Mode and Effect Analysis (FMEA) is popular technique for evaluating risk of failure modes of most industrial system. FMEA fundamentally carried out three functions. These are (Ben-Daya 2009): (1) to identify potential failures together with their causes and effects, (2) to estimate and rank identified failure modes and (3) to recommend actions to either mitigate or probably eliminate the chance of the potential failures from occurring. FMEA utilises RPN in estimating risk of failure and RPN is a product of three decision criteria; Occurrence of failure (O), Severity of the failure (S) and Detectability of the failure (D).

The application of the technique in evaluating risk have been reported in literature. Souza and Alvares (2008) proposed FMEA in conjunction with Fault Tree Analysis (FTA) as a risk assessment tool for application within the framework of Reliability Centred Maintenance (RCM). Cicek and Celik (2013) applied the FMEA in prioritising risk of crankcase failures of ship main engine. Cicek et al., (2010) used the approach to estimate risk of fuel oil system of marine diesel engine. Sankar and Prabhu (2000) applied FMEA to prioritise risk of failure of a cooling sub-system in an off-shore plant.

However, the conventional FMEA had been criticised in the literature to have

several limitations such as the inability to utilise more than three decision criteria in determining risk. On the basis of the limitations different enhanced FMEA approaches were developed and reported in the literature. For example, the Multi-Criteria Decision Making (MCDM) tool such as COPRAS, VOKOR and WSM had been applied in enhancing FMEA in the literature. Vahdani, (2015) utilised TOPSIS in enhancing FMEA for effective ranking of failure modes. Emovon et al., (2015) proposed the use of VIKOR technique for prioritising risk of failure modes of marine machinery system. In a similar research, Emovon (2016) applied integrated Dempster Shafer Theory and ELECTRE method for estimating risk of various equipment items of a marine diesel engine. Braglia, (2000) utilised AHP methodology in prioritising risk of failure modes. Sachdeva et al. (2009) used an integrated Shannon's entropy and TOPSIS techniques for risk assessment of a digester of a paper manufacturing plant in India. Zhao et al., (2017) proposed the use of MULTIMOORA combined with entropy for the ranking of failure modes.

Researchers have been much concerned about continuous improvement of ranking tools for effective risk prioritisation without considering the effectiveness of tools applied for aggregating data used as input into the ranking tools. There are basically two aggregating techniques commonly applied for aggregating failure modes ratings obtained from multiple experts. They are; Arithmetic Mean (AM) and

Geometric Mean (GM) techniques. In this paper a comparative analysis of the aforementioned methods is carried out in order to establish how they compare and their effects on the output of the ranking tools.

2. Methodology

2.1 Experts ratings aggregation methods

Averaging is the most frequently applied technique for combining inputs and it is regularly use in statistical analysis, multi-criteria decision making among others (Beliakov et al., 2016). In this paper, two most commonly used averaging function are considered for the aggregation of group experts ratings of failure modes (alternatives) in a group multi-criteria decision making process. They are; Arithmetic Mean (AM) and Geometric Mean (GM).

The ratings assigned by multiple experts which are tagged for aggregation are usually represented in the form of a decision matrix. The decision matrix formed as a result of z experts' ratings of failure modes i with respect to criteria j is expressed as:

$$P_{ij}^k = \begin{pmatrix} p_{ij}^k \\ p_{ij}^k \\ \dots \\ p_{ij}^k \end{pmatrix}_{m,n}, \quad k = 1, 2, \dots, z \quad i = 1, 2, \dots, m; \quad j = 1, 2, \dots, n \tag{1}$$

2.1.1 Arithmetic Mean (AM)

AM of the ratings assigned to alternative i based on certain criteria j by z number of experts can be expressed as:

$$x_{ij} = \frac{1}{z} \sum_{k=1}^z p_{ij}^k \tag{2}$$

2.1. 2 Geometric Mean (GM)

GM of the assigned ratings to alternative i with respect to criteria j by z number of experts can be expressed as follows:

$$x_{ij} = \sqrt[z]{\prod_{k=1}^z p_{ij}^k} \tag{3}$$

2.2 Ranking tools

2.2.1 FMEA

CEIEN 60812 Standard (2006) define FMEA as a methodology for industrial system analysis in order to identify potential failure modes and their corresponding effects on the performance of the system. FMEA uses RPN to estimate the risk contribution of each failure modes to the system and it is expressed as a product of probability of failure Occurrence (O), Severity of failure (S) and Detection of failure probability (D)

$$RPN = O \times S \times D \tag{4}$$

The ratings to O, S and D are commonly assigned by experts based on their judgement using a pre-determined scale. See an example in the work of Cicek and Celik (2013).

2.2.2 MCDM method

The most regularly used method for making decision involving more than one criteria is the Multi-Criteria Decision Making (MCDM) tool. There are many variant of the MCDM which include among others; VIKOR, TOPSIS, CP, WSM and WPS. The different types of MCDM tools have been applied in the literature in the modelling and solving diverse multi-criteria problems in various fields of human endeavour. In this paper; CP, VIKOR, WSM and WPM are applied as alternative to RPN of the FMEA in prioritising risk of failure modes.

2.2.2.1 Compromise Programming (CP)

In the year 1973 the CP method was proposed by Po-lung Yu and Milan Zeleny (Zeleny, 1982). The approach has since by applied in the literature in

addressing different multi-criteria decision problem. The aim is to obtain a solution that is closest to the ‘ideal’ solution. This can be achieved by comparing distances of different alternatives at various points to a particular reference point referred to as the ideal point. The alternative with the shortest distance to the reference point is the optimal solution. Diaz-Balteiro et al. (2011) proposed the use of CP technique for the ranking of seventeen European countries based on the sustainability of their paper industries. Amiri et al., (2011) used the approach for selection of portfolio based on 35 stock indices of Iranian stock market. Phua and Minowa (2005) applied the technique for forest conservation planning.

The steps involved in the CP analysis are as follows:

Step 1. The best and worst values evaluation for each criterion.

The best and worst values for each criterion are evaluated as follows:

$$x_{ij}^+ = \max_i x_{ij}, x_{ij}^- = \min_i x_{ij} \tag{5}$$

Where

x_{ij}^+ is the best value for j th criterion, and

x_{ij}^- is the worst value for the j th criterion.

Step 2. Evaluation of the performance index C_{pi}

The performance index is evaluated using the best and worst values as follows:

$$C_{pi} = \left[\sum_j w_j^p \left| \frac{x_{ij}^+ - x_{ij}^-}{x_{ij}^+ - x_{ij}^-} \right|^p \right]^{\frac{1}{p}} \tag{6}$$

Subject to $1 \leq p \leq \infty$

In this paper, the value of p was denoted as 2 because this is the value generally applied in the literature (Phua and Minowa, 2005; Zeleny, 1982).

The alternatives are ranked based on the performance index and the smaller the value the better the alternative.

2.2.2.2 VIKOR method

The VIKOR technique is an MCDM tool which selects a compromise solution using an index based on a measure of closeness to the positive ideal solution (Opricovic and Tzeng, 2004). The alternatives with the highest and lowest values with regard to risk criteria are the positive and negative ideal solutions respectively (Chu et al., 2007) while the optimum or compromise solution is the alternative farthest to the negative ideal solution. The application of the VIKOR technique in addressing different multi-criteria decision problems has been reported in the literature. Pamucar et al., (2017) applied the method to select the best location of a logistical center. Hsu et al., (2012) used the approach in the selection of vendors. Anojkumar et al., (2014) applied the technique in material selection problem.

The steps in the VIKOR analysis are as follows (Çalişkan et al., 2013):

Step 1. Determination of the utility measure and regret measure.

The best and worst values, determined using Equation 4 are applied as input data to determine utility and regret measures as follows:

$$U_i = \sum_{j=1}^n w_j (x_{ij}^+ - x_{ij}) / (x_{ij}^+ - x_{ij}^-) \tag{7}$$

$$V_i = \max_j [w_j (x_{ij}^+ - x_{ij}) / (x_{ij}^+ - x_{ij}^-)] \tag{8}$$

Where

w_j is the weight of j th criterion s

t_i is the utility measure

y_i is the regret measure

Step 2. Evaluation of the performance index Q_i ,

The performance index is expressed as:

$$Q_i = v(t_i - t^+) / (t^- - t^+) + (1-v)(y_i - y^+) / (y^- - y^+) \quad (9)$$

$$t^+ = \max_i [(t_i)], \quad i = 1, 2, \dots, m]$$

$$t^- = \min_i [(t_i)], \quad i = 1, 2, \dots, m]$$

$$y^+ = \max_i [(y_i)], \quad i = 1, 2, \dots, m]$$

$$y^- = \min_i [(y_i)], \quad i = 1, 2, \dots, m]$$

Where v can be any value from 0 to 1 and is generally set at 0.5 (Çalışkan et al., 2013). The ranking of the alternative is based on the performance index and the smaller the value the better the alternative.

2.2.2.3 Weighted Sum Model (WSM)

The WSM is the simplest form of MCDM technique and it utilises a linear relationship in the decision making process (Zardari et al., 2015). The approach have been applied in the literature in addressing various decision problem involving conflicting decision criteria. For example, Triantaphyllou and Mann, (1989) demonstrate the effectiveness of the approach using a numerical example.

The steps involves in the WSM analysis are (Chakraborty and Zavadskas, 2014):
Step 1: Normalisation of decision

The normalisation method depend on the type of criteria which is either beneficial or non-beneficial. The normalisation of the beneficial criteria

is carried out using the following expression:

$$z_{ij} = \frac{x_{ij}}{\max_i x_{ij}}, \quad j = 1, 2, \dots, n, \quad i = 1, 2, \dots, m \quad (10)$$

While the non-beneficial criteria normalisation is performed as follows:

$$z_{ij} = \frac{x_{ij}}{\min_i x_{ij}}, \quad j = 1, 2, \dots, n, \quad i = 1, 2, \dots, m \quad (11)$$

Step 2: Performance index evaluation

The performance index of alternative i^{th} using WSM is evaluated as follows:

$$Q_i = \sum_{j=1}^n z_{ij} w_j \quad (12)$$

The alternatives are ranked based on the evaluated performance index and the higher the value the better the alternative.

2.2.2.4 Weighted Product Model (WPM)

The WPM is a modified WSM designed in a way to avoid some of its limitations (Triantaphyllou and Mann, 1989).

The WPM begin with normalisation of the decision matrix using either Equations 9 or 10. The performance of alternative i^{th} is then evaluated as follows (Chakraborty and Zavadskas, 2014):

$$pQ_i = \prod_{j=1}^n (z_{ij})^{w_j} \quad (13)$$

The alternatives are ranked with respect to the performance index, pQ_i , and the optimal solution is the one with the highest value of pQ_i .

3. Case Study

To demonstrate the effectiveness of AM and GM techniques as tool for aggregating multi experts ratings of alternatives, comparative analysis was

conducted in search for better solution using a case study of fuel oil system of marine diesel engine of a ship system. Ten failure modes of the fuel oil system were identified for some equipment

items of the system. The failure modes together with the failure causes, effects of the failure and failure detection scheme of the system are presented in Table 1

Table 1 Failure modes of fuel oil system

FM #	Failure modes	Equipment items	Failure cause	Local effects	Global effects	Detection system
1	pipe leakage/rupture, sludge in fuel line	Fuel system-pipes, filter	deposits, low quality fuel oil	Hot spot , fuel oil spill	Stop engine, fire probable	Visual, high temperature deviation
2	Clogged fuel filter	Fuel system-pipes, filter	Contaminants, Lack of maintenance	Restriction in fuel flow (low fuel pressure), erratic cylinder firing	Engine speed drop, stop engine	Differential pressure alarm
3	Low supply pressure	High pressure fuel pump	Suction valve opens too early or late	Engine operates erratically	Reduced engine performance, stop engine	Low pressure alarm
4	Running without oil	Transfer/supply/Boster pump	Wear-out gear	Low supply pressure	Reduce output from engine	„
5	Abnormal sound	Transfer/supply/Boster pump	Bearing defective/ shaft displacement	Overloading of electric motor	Reduce output from engine	„
6	Fuel valve leaked	Fuel valve	Erosion, deposits	Excessive temperature after individual unit dropped	Reduce output from engine, hot spot	High exhaust temperature alarm
7	Seizure of injection valve spindle in open position	Fuel valve	Control system failure	Excessive fuel injected into the affected cylinder, high exhaust temperature, black smoke	Reduced engine performance, environmental damage	High exhaust temperature alarm

8	Fuel valve nozzle obstructed	Fuel valve	Inadequate maintenance, incorrect fuel temperature, contaminants, poor fuel quality	Poor combustion, discolored exhaust	Reduced engine performance, followed by engine failure	High exhaust temperature alarm
9	Early opening of fuel valve	Fuel valve	Low service pressure	Rough running, loss of compression and poor starting	Reduced engine performance	Low pressure alarm
10	Dripping	Fuel valve	Oversized injection mechanisms	Sticking of piston rings in their groove	Reduced engine performance, engine damage	High exhaust temperature alarm

For each of the failure modes, ratings assigned by three experts are presented in Table 2. Expert 1 rating in Table 2 were an agreed consensus rating of the ten failure modes from multiple experts

obtained from the work of Emovon (2016). Expert 2 and 3 ratings were generated to be within close range of Expert 1 ratings.

Table 2 Failure Mode Ratings

Failure modes	Expert 1			Expert 2			Expert 3		
	O	S	D	O	S	D	S	O	D
1	6	7	2	8	6	3	6	8	4
2	6	7	2	7	6	4	5	9	3
3	5	8	5	4	7	3	4	7	3
4	5	8	5	7	7	5	7	6	5
5	6	7	4	5	9	6	8	9	3
6	5	7	2	4	8	3	6	7	2
7	4	9	2	6	7	2	3	6	4
8	5	8	2	4	6	4	8	9	2
9	6	7	6	8	8	5	8	7	5
10	4	8	2	2	9	2	6	6	4

4. Case Study Analysis

4.1 Experts ratings aggregation

The experts' 1, 2 and 3 ratings in Table 2 are aggregated using Equations 2 and

3 to obtain AM and GM ratings of failure modes respectively and the results are shown in Table 3.

Table 3 AM and GM values of failure modes

Failure modes	AM			GM		
	O	S	D	O	S	D
1	6.6667	7.0000	3.0000	6.6039	6.9521	2.8845
2	6.0000	7.3333	3.0000	5.9439	7.2304	2.8845
3	4.3333	7.3333	3.6667	4.3089	7.3186	3.5569
4	6.3333	7.0000	5.0000	6.2573	6.9521	5.0000
5	6.3333	8.3333	4.3333	6.2145	8.2768	4.1602
6	5.0000	7.3333	2.3333	4.9324	7.3186	2.2894
7	4.3333	7.3333	2.6667	4.1602	7.2304	2.5198
8	5.6667	7.6667	2.6667	5.4288	7.5595	2.5198
9	7.3333	7.3333	5.3333	7.2685	7.3186	5.3133
10	4.0000	7.6667	2.6667	3.6342	7.5595	2.5198

The AM and GM ratings or values are then use as input into the different failure mode ranking techniques.

4.2 Comparative analysis of AM and GM

The AM and GM techniques are compared by inputting both aggregated ratings in Table 3 into each of the ranking tools; RPN, CP, VIKOR, WSM and WPM in turns to determine the similarity of the AM and GM data aggregation approach and their effect on the ranking tools.

4.2.1 Comparative analysis of AM and GM based on RPN

The AM and GM aggregated ratings of failure modes in Table 3 was used as input data in turns into Equation 4 to obtain RPN of failure modes of fuel oil system based on AM and GM respectively. The RPN of failure modes and corresponding ranking obtained based on AM and GM data are presented in Table 4.

Table 4 Comparison of AM and GM based on RPN failure modes rankings

FM #	AM					GM				
	O	S	D	RPN	Rank	O	S	D	RPN	Rank
1	6.6667	7.0000	3.0000	140.0	4	6.6039	6.9521	2.8845	132.4	4
2	6.0000	7.3333	3.0000	132.0	5	5.9439	7.2304	2.8845	124.0	5
3	4.3333	7.3333	3.6667	116.5	6	4.3089	7.3186	3.5569	112.2	6
4	6.3333	7.0000	5.0000	221.7	3	6.2573	6.9521	5.0000	217.5	2
5	6.3333	8.3333	4.3333	228.7	2	6.2145	8.2768	4.1602	214.0	3

6	5.0000	7.3333	2.3333	85.6	8	4.9324	7.3186	2.2894	82.6	8
7	4.3333	7.3333	2.6667	84.7	9	4.1602	7.2304	2.5198	75.8	9
8	5.6667	7.6667	2.6667	115.9	7	5.4288	7.5595	2.5198	103.4	7
9	7.3333	7.3333	5.3333	286.8	1	7.2685	7.3186	5.3133	282.6	1
10	4.0000	7.6667	2.6667	81.8	10	3.6342	7.5595	2.5198	69.2	10

The ranks of failure modes obtained based on AM and GM data are also presented in Figure 1. From Table 4 and Figure 1, Failure mode 1, 2, 3, 6, 7, 8, 9 and 10 have the same rank when both AM and GM data are applied as input data while Failure mode 4 and 5 have

one rank difference in between. From the comparative analysis, it is obvious that the ranking obtained for both AM and GM being applied as input data in RPN for the ranking of failure modes are almost completely the same.

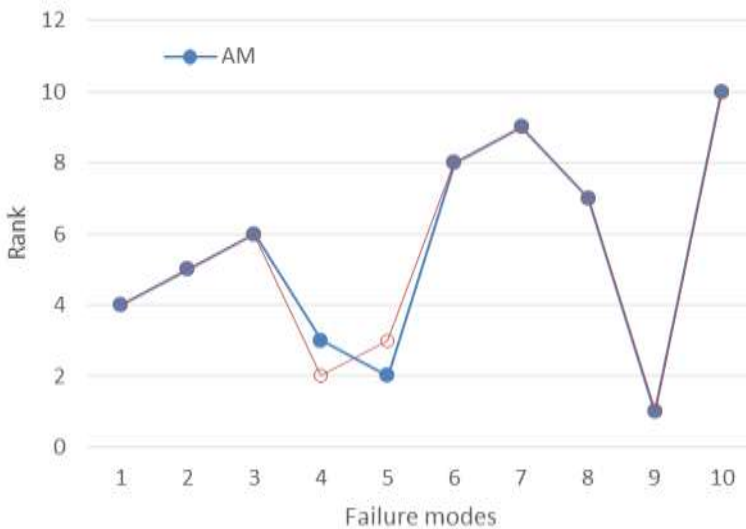


Fig. 1 Comparison of AM and GM based on RPN failure modes rankings

4.2.2 Comparative analysis of AM and GM based on CP

The first step in the comparative analysis of AM and GM is the determination of the weight of decision criteria; O, S and D. The entropy method was applied to estimate weights of decision criteria. The results for O, S and D are 0.3081, 0.0197 and 0.6722 respectively when AM data in Table 3 was applied into entropy methodology

while the weights for O, S and D are 0.3162, 0.0171 and 0.6667 respectively when GM data also in Table 3 are used as input data into entropy method. The CP performance index of the failure modes is then evaluated using Equation 5 and 6 on AM and GM decision matrix data in Table 3 and criteria weights. The performance index and corresponding rank obtained for failure modes based on AM and GM input data

are shown in Table 5. The ranks of failure modes obtained based on AM

and GM data are also presented in Figure 2.

Table 5 Comparison of AM and GM based on CP failure modes rankings

FM#	AM		GM	
	CP	Rank	CP	Rank
1	0.2768	5	0.2911	5
2	0.2859	6	0.3029	6
3	0.2024	4	0.2297	4
4	0.0129	2	0.0143	2
5	0.0572	3	0.0747	3
6	0.4900	10	0.4942	9
7	0.4199	8	0.4673	8
8	0.3765	7	0.4102	7
9	0.0002	1	0.0002	1
10	0.4345	9	0.4994	10

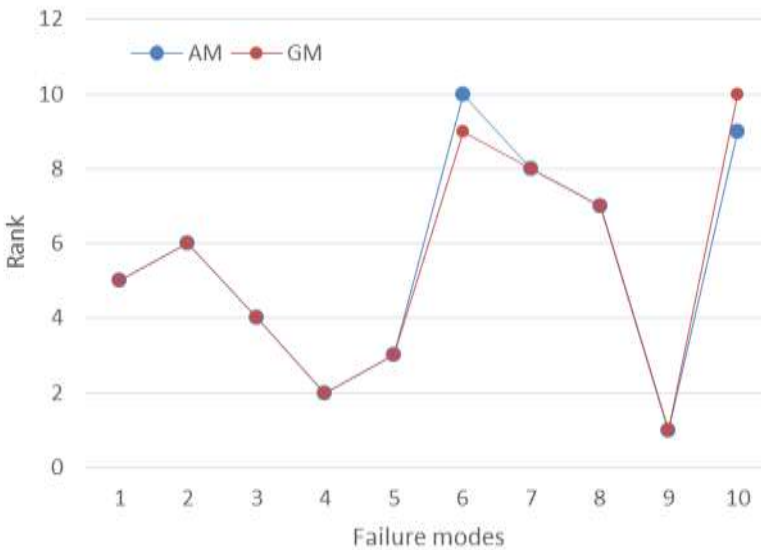


Fig. 2 Comparison of AM and GM based on CP failure modes rankings

From Table 5 and Figure 2, in almost all the failure modes, the same rank was obtained when both AM and GM data are applied as input data with the exception of failure mode 6 and 10 which has one rank difference in between. Again comparative analysis of AM and GM, showed that the ranking

of failure modes are almost completely the same when AM and GM data are used as input data.

4.2.3 Comparative analysis of AM and GM based on VIKOR

Using VIKOR method as the basis of comparison of AM and GM, firstly the best and worst values of failure modes

are determined using Equation 5 on AM and GM data in Table 3. This is followed by the determination of the utility and regret measures, by applying Equations 7 and 8 on the estimated decision criteria weights and the best and worst values. Finally, the performance index of each failure

modes based on AM and GM data are determined using Equation 9 and the results are presented in Table. Based on the performance index, the failure modes are ranked and the results for both AM and GM are compared as shown in Table 6.

Table 6 Comparison of AM and GM based on VIKOR failure modes rankings

FM #	AM		GM	
	Qi	Rank	Qi	Rank
1	0.7136	5	0.7216	5
2	0.7450	6	0.7506	6
3	0.6340	4	0.6335	4
4	0.1546	2	0.1448	2
5	0.3267	3	0.3644	3
6	0.9929	10	0.9682	10
7	0.9288	8	0.9388	8
8	0.8577	7	0.8771	7
9	0.0000	1	0.0000	1
10	0.9432	9	0.9612	9

From Table 6, same rankings of failure modes were obtained when both the AM and GM data were applied as input into the VIKOR technique.

4.2.4 Comparative analysis of AM and GM based on WSM

In comparing AM and GM based on WSM ranking of failure modes, the process starts with normalisation of decision matrix in Table 3 using Equation 10. The normalised matrix

and the evaluated decision criteria weights is then applied as input into Equation 12 to determined WSM performance index. The performance index and corresponding rankings obtained for failure modes when AM and GM aggregated data are used as input into WSM are presented in Table 7. The ranking of failure modes based on AM and GM data are also presented in Figure 4.

Table 7 Comparison of AM and GM based on WSM failure modes rankings

FM#	AM		GM	
	WSM	Rank	WSM	Rank
1	0.6776	7	0.6768	7
2	0.6504	5	0.6488	5
3	0.6650	6	0.6602	6
4	0.9175	9	0.9125	9
5	0.8360	8	0.8319	8
6	0.5237	1	0.5223	2
7	0.5380	3	0.5352	3
8	0.5948	4	0.5934	4
9	1.0027	10	0.9979	10
10	0.5248	2	0.5216	1

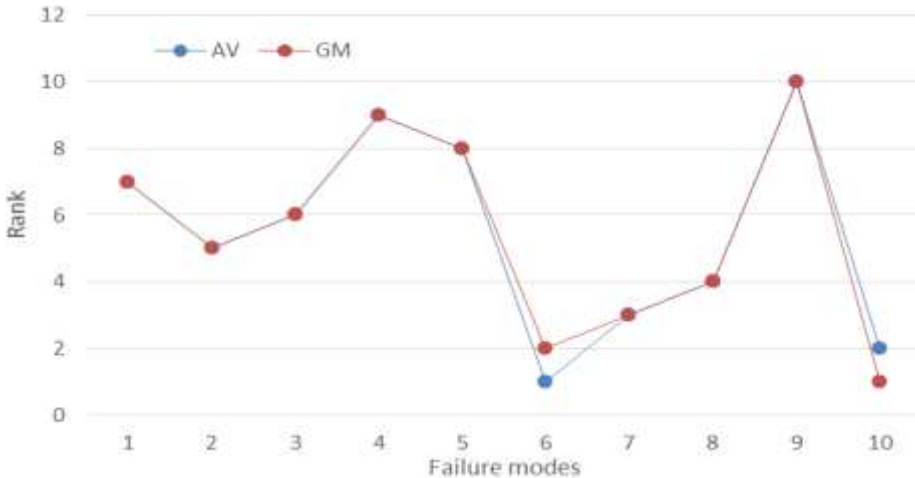


Fig 4 Comparison of AM and GM based on WSM failure modes rankings

From Figure 4, rankings obtained when AM and GM data are used as input into WSM are the same for failure modes 1,2,3,4,7 and 8 and slightly different for failure mode 5, 6, 9 and 10 with each having a rank difference of one between failure modes. Conclusively, ranking obtained for failure modes for both AM and GM data are relatively similar.

4.2.5 Comparative analysis of AM and GM based on WPM

To compare AM and GM methods based on WPM, decision matrix for

both AM and GM input data are normalised firstly. The normalised matrix and the evaluated decision criteria weights for AM and GM are applied as input into Equation 13 to produce WPM performance index for failure modes. The WPM performance index and corresponding rank for failure modes are shown in Table 8. The ranks for failure modes in both cases are also presented in Figure 5.

Table 8 Comparison of AM and GM based on WPM failure modes rankings

FM#	AM		GM	
	WPM	Rank	WPM	Rank
1	0.3257	6	0.3261	7
2	0.3156	5	0.3156	5
3	0.3267	7	0.3255	6
4	0.4520	9	0.4510	9
5	0.4120	8	0.4112	8
6	0.2520	1	0.2520	1
7	0.2638	3	0.2633	3
8	0.2868	4	0.2868	4
9	0.4943	10	0.4936	10
10	0.2576	2	0.2569	2

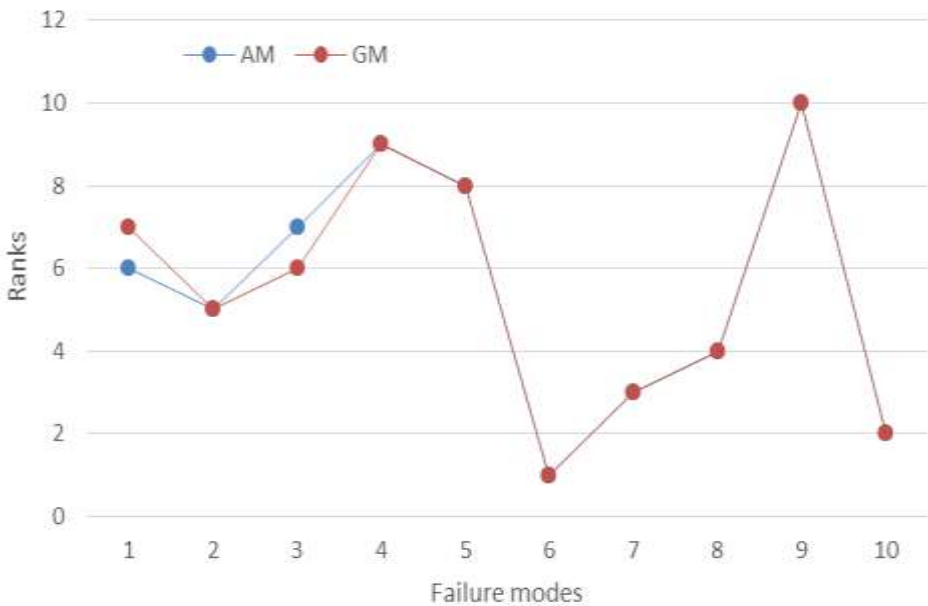


Fig 5 Comparison of AM and GM based on WPM failure modes rankings

From Figure 5, failure modes 2, 4, 5, 6, 7, 8, 9 and 10 representing 80% of the total failure have the same rank for both AM and GM aggregating technique while failure modes 1 and 3 representing 20% of the total failure modes have a difference of one rank in between failure modes. The rank

obtained in both scenario; AM and GM are almost completely the same.

5. Conclusion

In this paper two techniques are presented for the aggregation of experts assigned ratings for failure modes of marine machinery system. The two techniques are AM and GM. To

ascertain the effectiveness of the two approaches, a comparative analysis was performed in search of the better option using a case study of fuel oil system of marine diesel engine of a ship system. To achieve the paper objective, ratings assigned to failure modes of fuel oil system were aggregated with both AM and GM techniques. The aggregated ratings obtained by both methods were then used input data into RPN of FMEA, CP, VIKOR, WSM and WPM for the ranking of failure modes. The comparative analysis revealed that when AM and GM data are applied as input into RPN, CP and WPM, almost completely same ranking for failure modes were produced in both cases while when applied as input into VIKOR method, same result were generated for failure modes in both scenarios. However, when AM and GM data are applied as input into the WSM method significant difference in failure modes ranking were observed in both scenarios. Conclusively, the level of similarity between the AM and GM depend on the ranking tool applied for the prioritising failure modes. It can further be concluded, that VIKOR method is most stable of all the ranking methods having produced same ranking for failure modes irrespective of the aggregated data applied as input into the methodology.

References

- Amiri, M., Ekhtiari, M. and Yazdani, M., 2011. Nadir compromise programming: A model for optimization of multi-objective portfolio problem. *Expert Systems with Applications*, 38(6), pp.7222-7226.
- Beliakov, G., Sola, H.B. and Sánchez, T.C., 2016. A practical guide to averaging functions (Vol. 329). Heidelberg: Springer.
- Ben-Daya, M., 2009. Failure mode and effect analysis. In *Handbook of maintenance management and engineering* (pp. 75-90). Springer London.
- Braglia, M., 2000. MAFMA: Multi-attribute failure mode analysis. *International Journal of Quality and Reliability Management* 17 (9), 1017-1034.
- Çalışkan, H., Kurşuncu, B., Kurbanoglu, C., Güven, T.Y., 2013. Material selection for the tool holder working under hard milling conditions using different multi criteria decision making methods. *Materials and Design* 45, 473-479.
- Cicek, K. and Celik, M., 2013. Application of failure modes and effects analysis to main engine crankcase explosion failure on-board ship. *Safety Science*, 51(1), pp.6-10.
- Cicek, K., Turan, H.H., Topcu, Y.I. and Searslan, M.N., 2010, March. Risk-based preventive maintenance planning using Failure Mode and Effect Analysis (FMEA) for marine engine systems. In *Engineering Systems Management and Its Applications (ICESMA)*, 2010 Second International Conference on (pp. 1-6). IEEE.
- CEIEN 60812 Standard (2006), Analysis techniques for system reliability – Procedure for failure mode and effects analysis (FMEA).
- Chakraborty, S. and Zavadskas, E.K., 2014. Applications of WASPAS method in manufacturing

- decision making. *Informatica*, 25(1), pp.1-20.
- Chu, M.-T., Shyu, J., Tzeng, G.-H., Khosla, R., 2007. Comparison among three analytical methods for knowledge communities group-decision analysis. *Expert Systems with Applications* 33 (4), 1011-1024.
- Diaz-Balteiro, L., Voces González, R., Romero, C., 2011. Making sustainability rankings using compromise programming. An application to European paper industry. *Silva Fennica* 45 (4), 761-773.
- Emovon, I. (2016) Failure Mode and Effects Analysis Of Ship Systems using an integrated Dempster Shafer Theory And ELECTRE Method, *Journal of Advanced Manufacturing Technology*, 10(1), p45-60.
- Emovon, I., Norman, R.A., Murphy, A.J. and Pazouki, K., 2015. An integrated multicriteria decision making methodology using compromise solution methods for prioritising risk of marine machinery systems. *Ocean Engineering*, 105, pp.92-103.
- Hsu, C.H., Wang, F.-K., Tzeng, G.-H., 2012. The best vendor selection for conducting the recycled material based on a hybrid MCDM model combining DANP with VIKOR. *Resources, Conservation and Recycling* 66 (0), 95-111.
- Opricovic, S., Tzeng, G.H., 2004. Compromise solution by MCDM methods: A comparative analysis of VIKOR and TOPSIS. *European Journal of Operational Research* 156 (2), 445-455.
- Pamučar, D.S., Božanić, D. and Randelović, A., 2017. Multi-criteria decision making: An example of sensitivity analysis. *Serbian Journal of Management*, 12(1), pp.1-27.
- Phua, M.-H., Minowa, M., 2005. A GIS-based multi-criteria decision making approach to forest conservation planning at a landscape scale: a case study in the Kinabalu Area, Sabah, Malaysia. *Landscape and Urban Planning* 71 (2-4), 207-222.
- Ravi Sankar, N. and Prabhu, B.S., 2001. Modified approach for prioritization of failures in a system failure mode and effects analysis. *International Journal of Quality & Reliability Management*, 18(3), pp.324-336.
- Sachdeva, A., Kumar, P., Kumar, D., 2009. Maintenance criticality analysis using TOPSIS, 2009 IEEE International Conference on Industrial Engineering and Engineering Management, Hong Kong, pp. 199-203.
- Triantaphyllou, E. and Mann, S.H., 1989. An examination of the effectiveness of multi-dimensional decision-making methods: a decision-making paradox. *Decision Support Systems*, 5(3), pp.303-312.
- Vahdani, B., Salimi, M. and Charkhchian, M., 2015. A new FMEA method by integrating fuzzy belief structure and TOPSIS to improve risk evaluation process. *The International Journal of Advanced Manufacturing Technology*, 77(1-4), pp.357-368.
- Zardari, N.H., Ahmed, K., Shirazi, S.M. and Yusop, Z.B., 2015. Literature

- Review. In *Weighting Methods and their Effects on Multi-Criteria Decision Making Model Outcomes in Water Resources Management* (pp. 7-67). Springer International Publishing.
- Zeleny, M., 1982. *Multiple Criteria Decision Making*. McGraw-Hill.
- Zhao, H., You, J.X. and Liu, H.C., 2017. Failure mode and effect analysis using MULTIMOORA method with continuous weighted entropy under interval-valued intuitionistic fuzzy environment. *Soft Computing*, 21(18), pp.5355-5367.



Crevice Corrosion Behavior of Nickel-Based Alloy 718 in both Aerated and De-Aerated Chloride Environment

F. Bakare^{1,2}, J. Ugorji¹, Y. Alsubhi¹,
S. Okunzuwa² & A. Orobor³

¹School of Materials, University of Manchester,
Manchester, M13 9PL, United Kingdom

²Department of Physics, University of Benin,
Benin City, Edo, Nigeria

³Department of Mechanical Engineering, University of Benin,
Benin City, Nigeria

folarin.bakare@uniben.edu (Corresponding Author),

jarminugorji@gmail.com,

subhiys@aramco.com,

okunzuwas@yahoo.com,

awheme.oghenerobor@uniben.edu

Abstract: In this study, anodic potentiodynamic polarization techniques were used to study the crevice corrosion behaviour of Nickel alloy 718 (with and without a crevice former) in both aerated and de-aerated solution of 3.5wt% sodium chloride solution. Surface observation of the specimens after each experiment was done with the optical microscope. The results showed that crevice corrosion were initiated at potentials as low as 520mVSCE, while the surface observation on the specimen with a crevice former revealed that the crevice corrosion attack was restricted under the crevice gap and at the border areas of the crevice former but did not occur at the surfaces outside the shielded areas. Conversely, the specimen without a crevice former showed evidence of waterline corrosion. These results can be attributed to the development of differential oxygen concentration in the specimen

depending on the exposure of the parts to dissolved oxygen. This study has developed a more comprehensive understanding of the crevice corrosion initiation mechanism and behaviour of Nickel-based Alloy 718 under applied crevice torques, chloride environment and exact potentials, thereby leading to better prevention and control of localized corrosion in this alloy.

Keywords: Nickel-based alloy 718; localized corrosion; Crevice corrosion; polarization curve; crevice former;

1.0 Introduction

Nickel based alloy 718 has recently gained extensive use for constructing the downhole assembly of the drilling rig employed in the oil and gas industries due to its excellent combination of mechanical properties, corrosion resistance and non-magnetic properties [1-5]. In more details, the candidacy of alloy 718 for the downhole drilling activities has been attributed to the order strengthening of the γ'' - phase, precipitation hardening of γ' - particles in the γ -matrix and the balanced additions of Chromium (Cr) and Molybdenum (Mo) alloying elements, especially at temperatures as high as 650°C [6]. The alloying elements of Cr and Mo has been found to form dense oxide/hydroxide films when exposed to aqueous electrolytes or moist air [7]. However, the mechanical and electrochemical interaction between surfaces in relative motion and in the presence of corrosive environment (Tribocorrosion) typical of those encountered in drilling processes can remove the passive film, as a result, exposing the surface of the alloy substrate, thereby giving rise to anodic dissolution of the alloy. For instance, the presence of significant concentrations of chlorides, hydrogen sulphide (H_2S), carbon dioxide (CO_2) coupled with the high operating temperatures especially in the deeper wells of oil and gas exploration has greatly hampered the performance of

Nickel-based alloy 718, and has generated attention from researchers to mitigate or eliminate the failure of this alloy by pitting corrosion, crevice corrosion, environmental assisted cracking including hydrogen embrittlement and stress corrosion cracking [8-11]. Kehler et al [12] investigated the crevice corrosion stabilization of Nickel-based alloys (625 and 22) and concluded that it is been influenced by temperature and electrolyte composition but not by the pH of the bulk solution. Additionally, she successfully assessed the crevice corrosion resistance of these alloys by relating the voltage dependent crevice corrosion rate to the open-circuit potentials. McCoy and his colleagues [13] reviewed the materials selection of Nickel-based alloys on the basis of an excellent blend of mechanical and corrosion properties for simulated (sweet and sour) oilfield requirements. Hayes et al [14] performed a post-localized breakdown analysis by introducing Cr and Mo in specified amounts to Nickel-based alloy and noticed that the passivity of the alloy was maintained and stabilized after a localized breakdown event. Mishra et al [15] determined the crevice re-passivation potential and temperature for Alloy 22 (UNS06022) using Tsujikawa-Hisamatsu electrochemical technique (THE). Amin et al [16] attempted and succeeded to reduce the tribocorrosion issues in Nickel-based alloy 718 by adding about 2.5-3.5% amount of Rhenium (Re) to the matrix.

It was pointed out that 6% additions only increased the rate of uniform and pitting corrosion processes. Mishra et al [17] studied the role of alloying elements in a number of commercially available Nickel-based alloys under several aggressive environments by evaluating the weight loss, electrochemical changes and surface characterization techniques. Due to the scarce literature of the corrosion behaviour between air and anaerobic conditions in the presence of chloride ions. The study of the corrosion kinetics in the above mentioned environment could prove useful due to the difference in oxygen concentration as the depth of downhole drilling increases. Consequently, there is need to study the crevice corrosion behaviour of this

alloy in different microstructural conditions under a synergistic simulated corrosive environment of chloride ions in both aerated and de-aerated form in order to separate the effect of oxygen from the rate of rotation as a result of applied torque and to analyze the corrosion kinetics by surface characterization and anodic potentiodynamic polarization techniques.

2.0 Materials and Methods

Commercial Nickel-based alloy 718 (UNS N07718) samples with dimensions of 19.73x19.73x2.44mm in the mill-annealed condition were used in this experiment. The chemical composition of the alloy is shown in Table 1 below.

Table 1: Nominal composition of Nickel-based Alloy 718 [18].

Element	Al	C	Co	Cr	Cu	Fe	Mo	Ti	Nb	Ni
mass %	0.52	0.021	0.11	19.06	0.02	18.15	3.04	0.93	5.08	53.0

For the electrochemical experiments, a stainless steel wire was spot welded to the specimens to establish an electrical connection with the specimen. This was then covered with a plastic tube, held to the spot welded area with an adhesive and the uncovered surface area of the spot weld was coated with a protective epoxy resin to prevent electrical conductivity and formation of fine crevices. The crevice assembly consists of a steel metal fastener (Nut and bolt with washers) to secure the crevice assembly and a crevice former with dimension (outer diameter – 16.02mm, inner diameter – 4.06mm and thickness – 6.40mm). Potentiodynamic polarization in 3.5% NaCl solution was

carried out in both aerated and de-aerated condition. The specimens were used as the working electrode while a platinum electrode and saturated calomel electrode (SCE) were used as counter and reference electrode respectively. The three electrodes were appropriately connected to the Potentiostat (Ivium Compactstat) whose output data was digitally recorded on the computer software (Iviumsoft). Two tests were carried out for each set of experiments at room temperature with aeration; one test specimen without crevice assembly and the other with crevice assembly to actually ascertain the effect of crevice former (crevice torque applied) and the potential at

which crevice corrosion initiates on the alloy in this particular test environment. A total of three sets of experiments were carried out with different crevice torques applied (0.5Nm, 1.0Nm and 1.5Nm respectively). Before the potentiodynamic scans were conducted, the test specimens were allowed to stabilize in the test solution at open-circuit for 120s. The potentiodynamic polarization scans were conducted from 300mVSCE below the open-circuit Potential, E_{ocp} in the anodic direction with scan rate of 1mV/s and limiting current density of 100 $\mu\text{A}/\text{cm}^2$. The sweeps was set to end in the forward direction without reversing when the potential reaches 1500mVSCE.

The crevice corrosion potential E_{crev} was identified as the point at which crevice corrosion initiates (the point at which there is an increase in current), to enable effective analysis and understanding of the crevice corrosion behaviour of alloy 718 in chloride environment. The same set of experiments described above were carried out but in de-aerated environment where a constant flow of nitrogen gas was bubbled into the solution for about 30minutes to reduce the dissolved oxygen concentration in the solution before the start of the potentiodynamic polarization scan and the flow rate was reduced and maintained until the end of the scan. The same crevice torque of 1.5Nm was used for the four sets of experiments while the scan started 300mVSCE below the open-circuit potential and final point of the scans were set at 300mVSCE, 1200mVSCE and 1500mVSCE respectively. This was to actually ascertain the effect of the various potentials on the surface of the specimen and the potential at which at

which crevice corrosion starts to initiate. After each experiment, the specimens were dismantled, allowed to dry for 10minutes and visualized using the OLYMPUS optical microscope with $\times 5$ magnification.

3.0 Results

3.1 Potentiodynamic polarization in aerated 3.5wt% sodium chloride (NaCl) with and without crevice former

The potentiodynamic polarization scan was done at various set potentials to produce a reproducible results to develop the standard electrochemical parameters to image the crevice corrosion behaviour of Nickel alloy 718 (UNS N07718).

Fig. 1 shows the potentiodynamic polarization scan results obtained where the final scan points were set at 300mVSCE, 600mVSCE, 900mVSCE, 1200mVSCE and 1500mVSCE respectively. However for a clearer analysis of the plot, Fig. 2 which shows the potentiodynamic polarization scan at final scan point of 1200mVSCE and applied crevice torque of 1.5Nm was concentrated upon. It can be observed that the specimen exhibits passive behaviour at the early stages of the potentiodynamic polarization scan until at about 520mVSCE and limiting current density of $10^{-5.8}\text{A}/\text{cm}^2$. Although corrosion was observed in both specimens with the crevice former and those without the crevice former, corrosion on the specimen without the crevice former seems to be waterline corrosion. As the potential increased in the anodic direction, the passive region remained constant until about the potential of 520mVSCE when there was a sharp increase in the current density from $10^{-5.8}\text{A}/\text{cm}^2$ to $10^{-4.3}\text{A}/\text{cm}^2$.

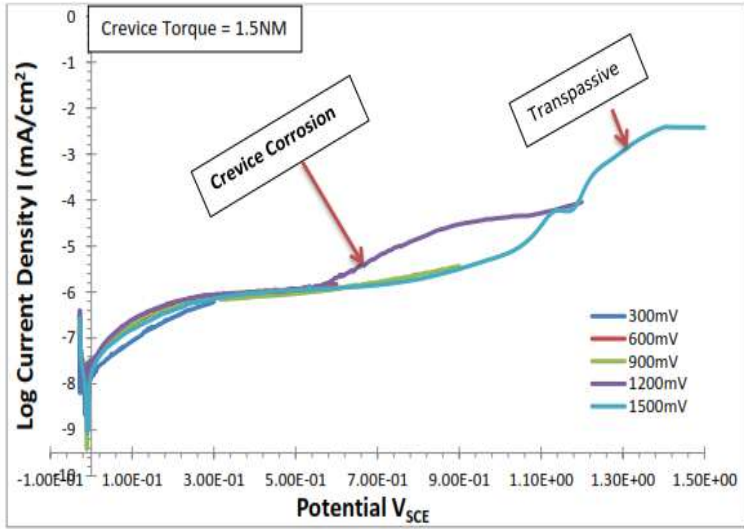


Fig. 1: Potentiodynamic polarization scan in aerated solution of 3.5wt% sodium chloride with crevice former at final scan point of 300mV_{SCE},

600mV_{SCE}, 900mV_{SCE}, 1200mV_{SCE} and 1500mV_{SCE} and crevice torque of 1.5Nm

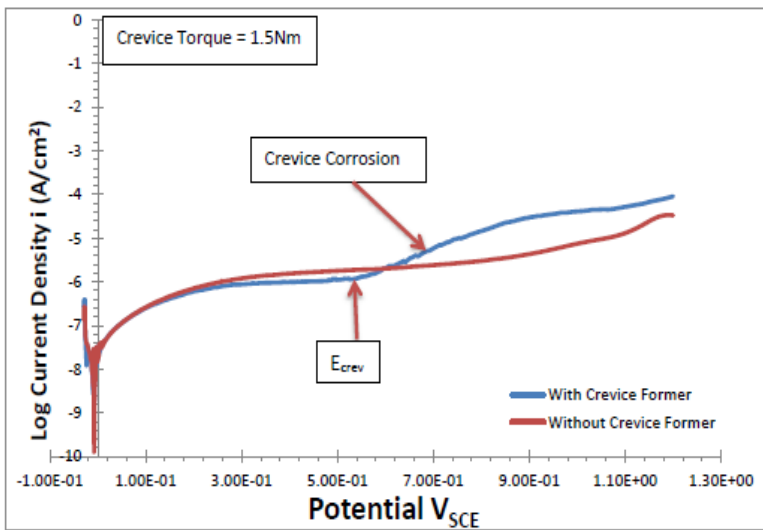


Fig. 2: Potentiodynamic polarization scan in aerated solution of 3.5wt% sodium chloride with and without crevice former at final scan point of 1200mV_{SCE} and applied crevice

torque of 1.5Nm showing crevice corrosion attack on the specimen.

Fig. 3 shows the optical micrographs of the various specimens (with and without a crevice former) of nickel alloy 718 after potentiodynamic

polarization in 3.5wt% aerated sodium chloride solution at (a) 1500mVSCE (b) 1200mVSCE, (c) 900mVSCE (d) 600mVSCE (e) 300mVSCE. Although there were no traces of crevice corrosion between 300-900mVSCE, but some form of artefacts were present probably due to either surface grinding or surface etching resulting from poor sample preparation. Crevice starts to

initiate at the border area of the crevice former but did not develop at either the inner surface of the shielded area by the crevice former or the surface outside the crevices at scan points of 1200mVSCE. Corrosion attack was also observed on specimens without the crevice former at the final point scan of 1500mVSCE mainly at the water-line area

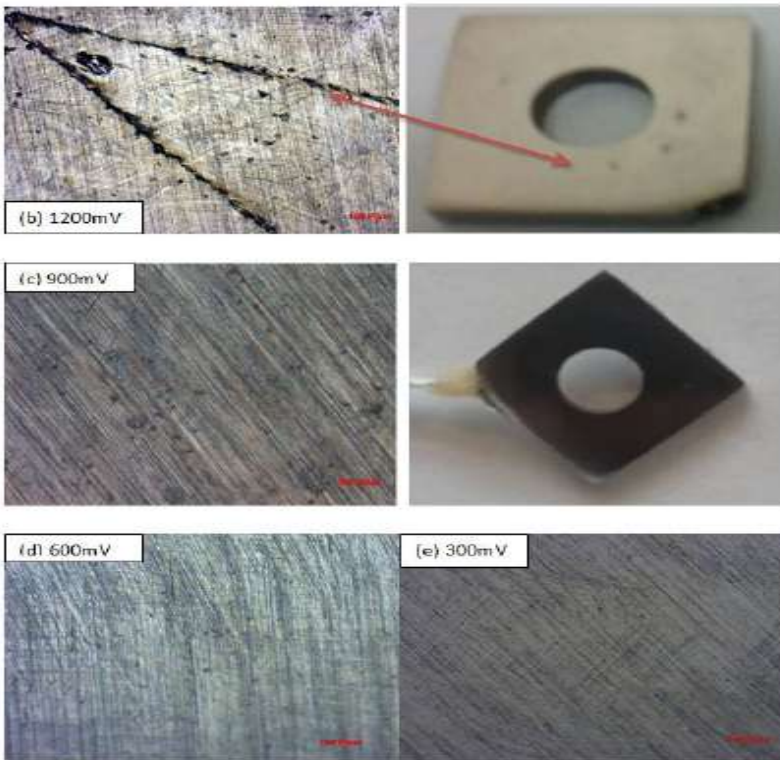


Fig. 3: Optical surface examination of nickel alloy 718 specimen with crevice former after potentiodynamic polarization in 3.5wt% aerated sodium chloride solution at (a) 1500mVSCE (b) 1200mV SCE, (c) 900mVSCE (d) 600mVSCE (e) 300mVSCE.

Fig. 4 shows the optical micrographs of nickel alloy 718 without a crevice former after potentiodynamic

polarization in 3.5wt% aerated sodium chloride solution at (a) 1500mVSCE (b) 1200mV SCE (c) 900mVSCE, (d) 600mVSCE, and (e) 300mVSCE respectively. The waterline corrosion was visible only at the potential of 1500mVSCE and not for 1200mVSCE, 900mVSCE, 600mVSCE, 300mVSCE respectively

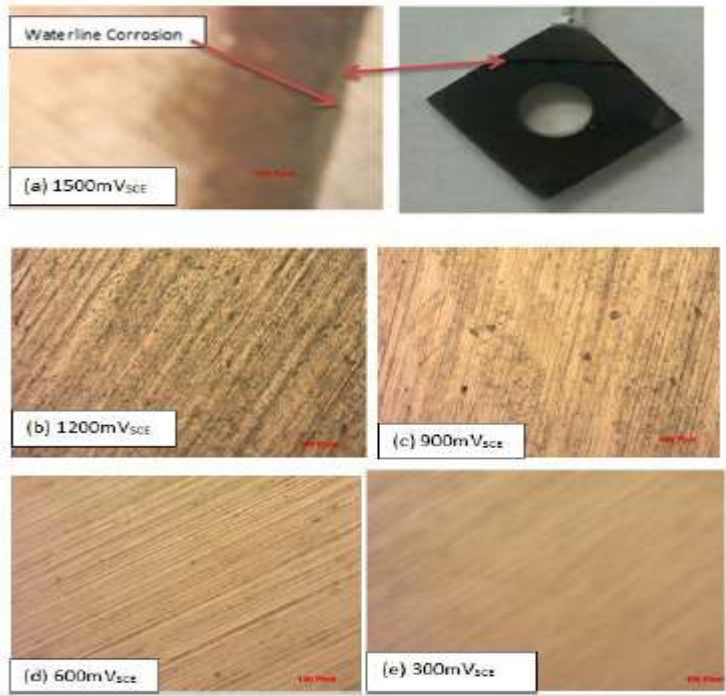


Fig. 4: Optical micrographs of nickel alloy 718 specimen without crevice former after potentiodynamic polarization in 3.5wt% aerated sodium chloride solution at (a) 1500mV_{SCE} (b) 1200mV_{SCE} (c) 900mV_{SCE} (d) 600mV_{SCE} and (e) 300mV_{SCE}.

3.2 Potentiodynamic polarization in de-aerated 3.5wt% sodium chloride (NaCl) with and without crevice former and at different scan points

The same sets of experiments discussed earlier were conducted but in the de-aerated solution with and without crevice former and at final point scans of 300mV_{SCE}, 1200mV_{SCE}, and 1500mV_{SCE}.

The potentiodynamic polarizations scan in de-aerated solution of 3.5wt% sodium chloride at different scan points (Fig. 5 and 6), with and without a crevice former (Fig. 7) is presented below. In the presence of a crevice

former, crevice corrosion was observed at final scan point of 1500mV_{SCE}. It will be observed from the graph that the crevice corrosion initiated (E_{crev}) was at the potential of about 530mV_{SCE}, which is approximately the same point in the aerated environment. Whereas in the absence of crevice former, the increase in current observed on the graph as pictured in Fig. 6 is at the potential of about 870mV_{SCE}. No crevice corrosion was observed at final scan points of 1200mV_{SCE} and 300mV_{SCE} as shown in Fig. 6 below. In Fig. 7, a rapid increase in current which coincides with crevice corrosion initiation above the passive current density were observed at about a potential of 530mV_{SCE} at final scan points of 1500mV_{SCE} as found in the aerated environment, but with a difference in potential of about 10mV_{SCE} on comparison with Fig. 2 above.

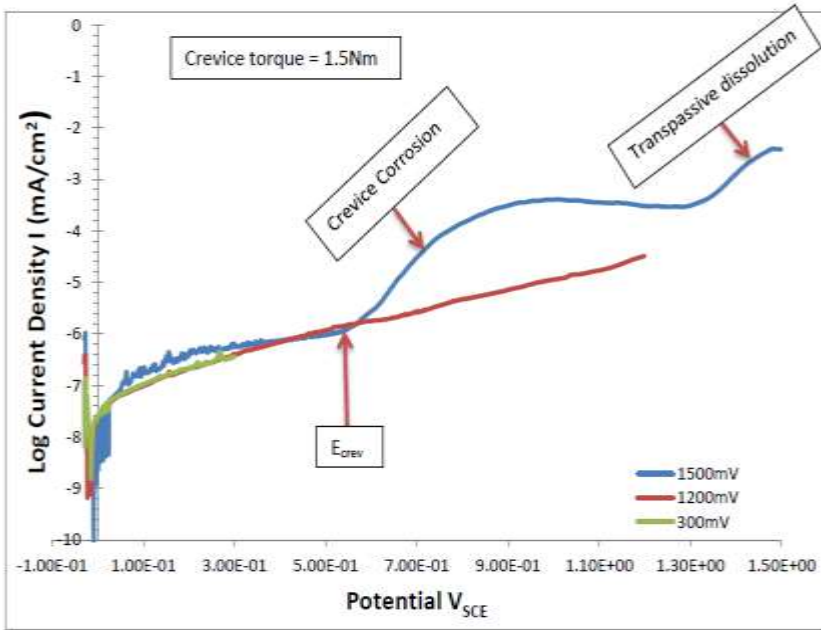


Fig. 5: Potentiodynamic polarization scan in deaerated solution of 3.5wt% sodium chloride with crevice former at final scan point of 1500mV_{SCE}, 1200mV_{SCE} and 300mV_{SCE}

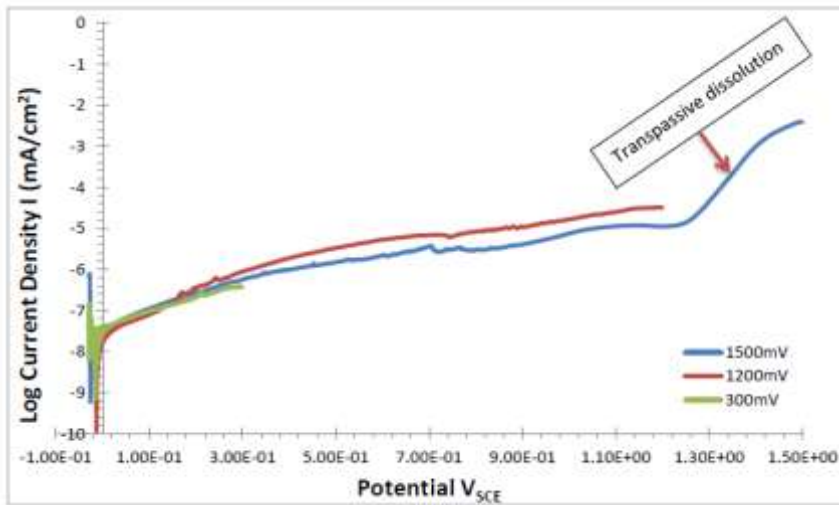


Fig. 6: Potentiodynamic polarization scan in deaerated solution of 3.5wt% sodium chloride without crevice former at final scan point of 1500mV_{SCE}, 1200mV_{SCE} and 300mV_{SCE}

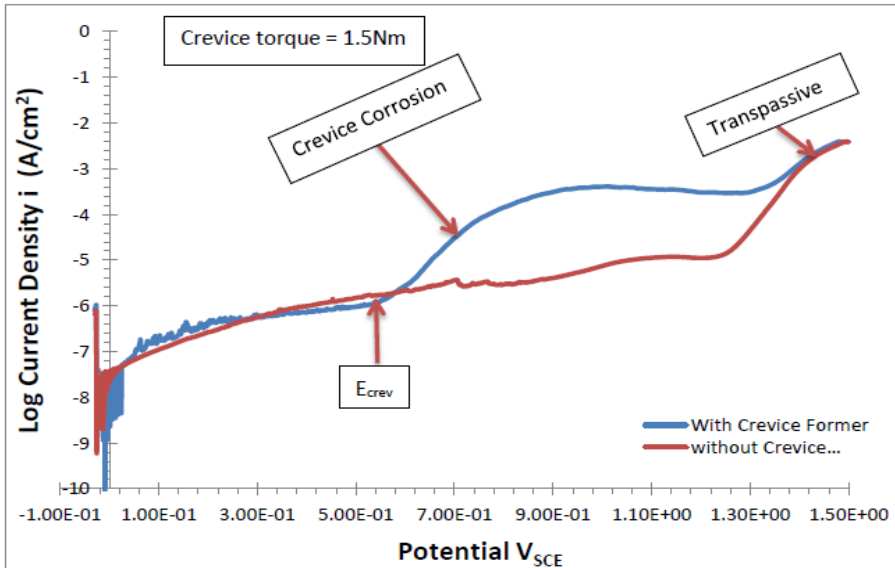


Fig. 7: Potentiodynamic polarization scan in deaerated solution of 3.5wt% sodium chloride with and without crevice former at final scan point of 1500mVSCE

The surface examination of the test specimens were carried out as shown in Fig. 8 and 9. When a crevice former is present as shown in Fig. 8, crevice corrosion was observed at final scan point of 1500mVSCE which correlates with the result shown on the potentiodynamic polarization plot in Fig. 5 and 6. Additionally, crevice corrosion was seemingly initiating at final scan point of 1200mVSCE but this was not evident in the polarization plot. The black de-colouration could probably be some form of artefact due to either surface grinding or surface etching resulting from the crevice

corrosion process. There was no evidence of crevice corrosion at final scan point of 300mVSCE. Fig. 9 shows the surface examination (Optical microscopy) of nickel alloy 718 specimen without crevice former after potentiodynamic polarization in 3.5wt% de-aerated sodium chloride solution at 1500mVSCE (b) 1200mV SCE and (c) 300mVSCE. Some little forms of transpassive metal dissolution were observed at the final scan point of 1500mVSCE and there was no evidence of corrosion at final scan point of 1200mVSCE and 300mVSCE respectively.

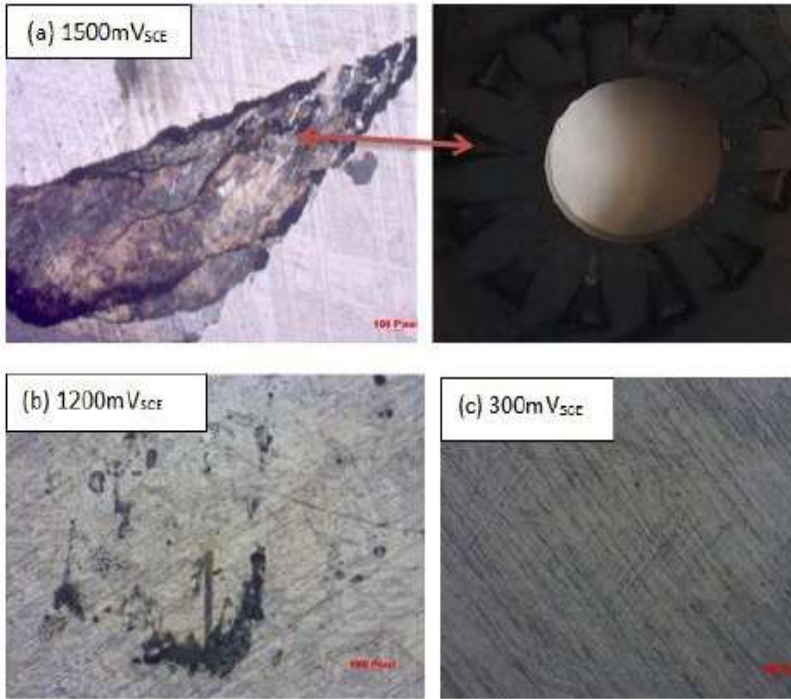


Fig. 8: Optical micrograph of nickel alloy 718 specimen with crevice former after potentiodynamic polarization in 3.5wt% de-aerated sodium chloride solution at 1500mV_{SCE} (b) 1200mV_{SCE} and (c) 300mV_{SCE}.

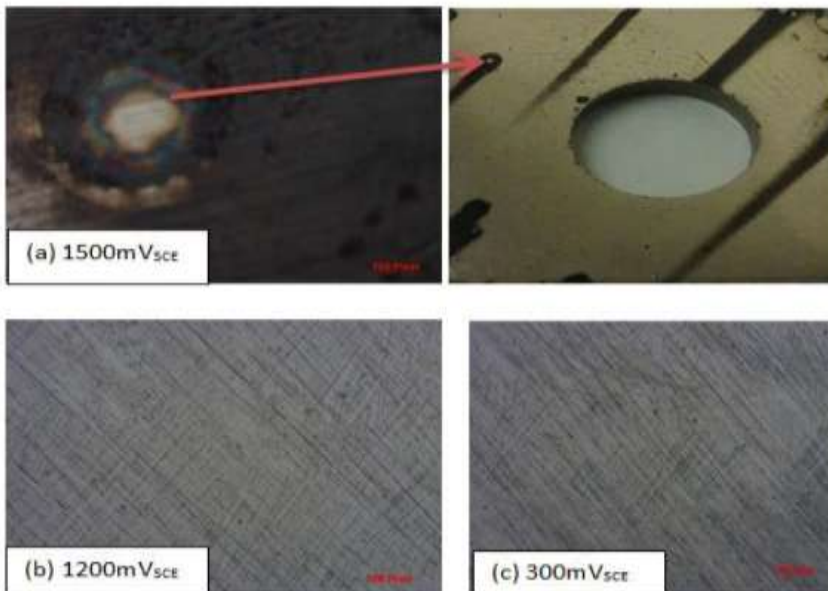


Fig. 9: Optical micrographs of nickel alloy 718 specimen without crevice former after potentiodynamic polarization in 3.5wt% de-aerated sodium chloride solution at 1500mV_{SCE} (b) 1200mV_{SCE} and (c) 300mV_{SCE}

4.0 Discussion

The sharp increase in the current density as observed in Fig. 1 is an evidence of crevice corrosion in the aerated solution of 3.5wt% sodium chloride with crevice former where the final scan point was set 1200mVSCE and applied crevice torque of 1.5Nm. The waterline corrosion in the sample without the crevice former could be attributed to the development of a differential oxygen concentration cell as suggested by Palanna [20] and subsequent deposition of electrons (rust) at the waterline area. The part of the specimen immersed lower in the solution (anode) is exposed only to less dissolved oxygen than the part higher in the solution (cathode), which is in direct contact with atmospheric oxygen. This causes corrosion to take place at the anode while the cathode is free from corrosion.

The corrosion initiation at scan points of 1200mVSCE in the presence of a crevice former conforms to the fact that crevice corrosion initiates preferentially from the crevice mouth (border area of crevice former) and moves towards the centre of the crevice former according to [21] at this particular potential. This also validates that crevice corrosion does not occur outside crevices as opined by Rashidi et al [22]. In the absence of crevice former, the visible waterline corrosion only at the potential of 1500mVSCE and not for 1200mVSCE, 900mVSCE, 600mVSCE, 300mVSCE respectively is due to differential aeration as discussed earlier.

The current increase observed in Fig. 5 could be attributed to the transpassive metal dissolution of the alloy. This was not observed at final scan point of

300mVSCE and 1200mVSCE because the potentials were not high enough to cause transpassivity.

5.0 Conclusion

The crevice corrosion behaviour of Nickel based alloy (Alloy 718 UNS N07718) in 3.5wt% sodium chloride has been studied using the potentiodynamic polarization electrochemical method. The microscopic observation of the surface of the alloy after each of the experiments was conducted. The following conclusions can be drawn:

1. Crevice corrosion was observed to occur on the specimen with a crevice former in aerated solution of 3.5wt% of sodium chloride from the polarization curve.
2. The surface observation with the optical microscope revealed that crevice corrosion attack was restricted under the crevice gap and at the border areas of the crevice former but did not occur at the surfaces outside the shielded areas, which shows the effect of the crevice former on crevice corrosion initiation of nickel-based alloy 718 (UNS N07718).
3. Waterline corrosion occurred on the specimens partially immersed into the solution of 3.5wt% of sodium chloride without a crevice former. This can be attributed to the development of a differential oxygen concentration.
4. This study can be used to validate the fact that crevice corrosion is a stochastic process as pointed out by Schweitzer et al [9] and can occur at potentials as low as 520mVSCE. Moreover, It will guide the development of standard electrochemical parameters to image the crevice corrosion behaviour of Nickel alloy 718 (UNS N07718).

References

- [1] Onyewuenyi, O., 1989. Alloy 718-- Alloy Optimization for Applications in Oil and Gas Production. *Superalloy 718: Metallurgy and Applications*, pp.345-362.
- [2] Slama, C. and Abdellaoui, M., 2000. Structural characterization of the aged Inconel 718. *Journal of alloys and compounds*, 306(1), pp.277-284.
- [3] Bhavsar, R. B., Collins, A., & Silverman, S. (2001). Use of alloy 718 and 725 in oil and gas industry. *Minerals, Metals and Materials Society/AIME, Superalloys 718, 625, 706 and Various Derivatives(USA)*, 47-55.
- [4] Yin, Z.F., Zhao, W.Z., Lai, W.Y. and Zhao, X.H., 2009. Electrochemical behaviour of Ni-base alloys exposed under oil/gas field environments. *Corrosion Science*, 51(8), pp.1702-1706.
- [5] Chen, T., John, H., Xu, J., Lu, Q., Hawk, J. and Liu, X., 2014. Influence of surface modifications on pitting corrosion behavior of nickel-base alloy 718. Part 2: Effect of aging treatment. *Corrosion Science*, 78, pp.151-161.
- [6] Hertweck, B., Steigerwald, T.G., Alt, N.S. and Schluecker, E., 2014. Different corrosion behaviour of autoclaves made of nickel base alloy 718 in ammonobasic and ammonoacidic environments. *The Journal of Supercritical Fluids*, 95, pp.158-166.
- [7] Zhang, X. and Shoesmith, D.W., 2013. Influence of temperature on passive film properties on Ni–Cr–Mo Alloy C-2000. *Corrosion Science*, 76, pp.424-431.
- [8] Behrens, R. and Agarwal, D.C., 2005, January. Laboratory Testing Of Age-Hardenable Alloys Environments 925 And 718 In Sour Gas: Proc. of Corrosion 2005 Conf., Houston, Texas: NACE Int., 2005, Paper No. 05103. .
- [9] Aberle, D. and Agarwal, D.C., 2008, January. High performance corrosion resistant stainless steels and nickel alloys for oil & gas applications: Proc. of Corrosion 2008 Conf., Houston, Texas: NACE Int., 2008, Paper No. 08085
- [10] Macdonald, K.A. and Bjune, J.V., 2007. Failure analysis of drillstrings. *Engineering Failure Analysis*, 14(8), pp.1641-1666.
- [11] Antunes, R.A. and de Oliveira, M.C.L., 2012. Corrosion fatigue of biomedical metallic alloys: mechanisms and mitigation. *Acta biomaterialia*, 8(3), pp.937-962.
- [12] Kehler, B.A., Ilevbare, G.O. and Scully, J.R., (2001). Crevice corrosion stabilization and re-passivation behavior of Alloy 625 and Alloy 22. *Corrosion*, 57(12), pp.1042-1065.
- [13] McCoy, S. A., Hereford, U. K., Puckett, B. C., Hibner, E. L., & Huntington, W. V. (2002). High performance age-hardenable nickel alloys solve problems in sour oil and gas service. *Balance*, 14(5), 16-23.
- [14] Hayes, J.R., Gray, J.J., Szmodis, A.W. and Orme, C.A., 2006. Influence of chromium and molybdenum on the corrosion of nickel-based alloys. *Corrosion*, 62(6), pp.491-500.
- [15] Mishra, A.K. and Frankel, G.S., 2008. Crevice corrosion repassivation of alloy 22 in

- aggressive environments. *Corrosion*, 64(11), pp.836-844.
- [16] Amin, M.A., El-Bagoury, N., Saracoglu, M. and Ramadan, M., 2014. Electrochemical and Corrosion Behavior of cast Re-containing Inconel 718 Alloys in Sulphuric Acid Solutions and the Effect of Cl. *Int. J. Electrochem. Sci*, 9, pp.5352-5374.
- [17] Mishra, A., Shoosmith, D. and Manning, P., 2016. Materials Selection for Use in Concentrated Hydrochloric Acid. *Corrosion*, 73(1), pp.68-76.
- [18] Thomas, A., El-Wahabi, M., Cabrera, J. M., & Prado, J. M. (2006). High temperature deformation of Inconel 718. *Journal of materials processing technology*, 177(1), 469-472.
- [19] Ren, X., Sridharan, K., & Allen, T. R. (2007). Corrosion behavior of alloys 625 and 718 in supercritical water. *Corrosion*, 63(7), 603-612.
- [20] Palanna, O. G. (2009). *Engineering chemistry*. Tata McGraw-Hill Education.
- [21] He, X., & Dunn, D. S. (2007). Crevice corrosion penetration rates of alloy 22 in chloride-containing waters. *Corrosion*, 63(2), 145-158.
- [22] Rashidi, N., Alavi-Soltani, S. R., & Asmatulu, R. (2007). Crevice corrosion theory, mechanisms and prevention methods.
- [23] Schweitzer, P. A. (1996). *Corrosion Engineering Handbook, -3 Volume Set*. CRC Press.



Suitability of some Selected Ado-Ekiti (Nigeria) Natural Moulding Sands' Properties for Sand Casting

¹Shuaib-Babata Y. L., ²Yaru S. S., ³Abdulkareem S.,
⁴Ajayi S., ⁵Busari Y. O., ⁶Ajao K. S., ⁷Ibrahim H. K.,
⁸Ambali I. O. & ⁹Mohammed G. A.

^{1,5,6,8}Department of Materials & Metallurgical Engineering,
University of Ilorin, Ilorin, Nigeria

²Department of Mechanical Engineering,
Federal University of Technology, Akure, Nigeria

^{3,7,9}Department of Mechanical Engineering,
University of Ilorin, Ilorin, Nigeria

⁴Department of Mechanical Engineering,
The Federal Polytechnic, Ado-Ekiti, Nigeria

sylbabata@gmail.com,

Shuaib-babata.yl@unilorin.edu.ng,

Abstract: In achieving accelerated and sustaining economic growth and development in Nigeria, there is need for domestication of finished goods production through sustainable industrialization. Foundry technology is one of the vital bases for rapid industrial development of any nation. Samples of moulding sand at green state were collected from four different moulding sand deposits within Ado-Ekiti in Nigeria. The samples were prepared using ASTM and British standards, while the materials' Physico-mechanical properties were evaluated using American Foundry Society (AFS)

guidelines. The results obtained from the tests were compared with the AFS's satisfactory mould sand properties for various types of metal castings. The sand samples were found to meet the requirements for casting various metals of different types like Aluminum, brass and bronze, light and malleable iron, light and medium grey iron, except heavy steel. The presence of red oxide in the sands and the specimens' higher compressive strength values show that the natural sands will be suitable for casting of non-ferrous metal of low temperature. Effective application of the sample sands in casting will also enhance industrialization, job creation and the nation self-reliance through reduction in importation of foundry sand and foundry products into the country.

Keywords: Casting, Moulding, Industrialization, Importation, goods and Mineral-resources

1.0 Introduction

Nigeria over dependence on importation of goods (such as ceramic wares, automobile parts, building materials, laboratory equipment, among others) to meet its citizenry needs has negatively affected the nation's economy [1, 2]. Different varieties of imported goods (durable and non-durable; new or fairly used) filled Nigeria markets, which makes locally produced goods to be seen as inferior goods [2]. Economy situation of the country has resulted to high rate of unemployment, hardship and poverty [3]. Nigeria's economy has been in recession for good five quarters with the negative growth recorded as revealed recently by the National Bureau of Statistics (NBS) [4]. Several researchers attributed the cause of this significant nation's problem to include over dependence on oil and gas sector, heavy importation of goods to meet its citizenry needs, and negligence on other economic sectors, like inadequate exploitation of available mineral resources, and poor industrialization [1,5,6,7,8].

Industrialization is significant to reduce over dependence of a nation on foreign goods and enhance export base [9]. According to Seipati and Itumeleng, "if production is subject to increasing

returns, export growth becomes a continual source of productivity growth" [10]. Exportation of locally produced goods to other countries makes a nation not to be commodity dependent economy. This will enable the nation to participate actively in international trade. Nigeria's participation in international trade has yielded tremendous contribution in productivity of domestic industries and advancement of the nation's technology [10, 11, 12]. Seipati and Itumeleng assume that "if a poor and smaller country can trade, there is some prospect of industrialization and of dispensing with traditional methods of production" [10].

To achieving accelerated and sustaining long economic growth and development in Nigeria, there is need for domestication of finished goods productions through industrialization at high rates, which will boost the nation's exportation. Osondu's opinion is that "there is no other route to achieving a national sustainable economic growth other than to find the appropriate ways to diversify the export base" [13]. This can be easily achieved through Industrialization with proper usage of available mineral resources like natural moulding sands, which Nigeria is greatly blessed with. Studies have

shown that Nigeria is well blessed with variety of natural resources like moulding sands, clay, gold, bronze, agricultural products, among others, which are not adequately utilized [14,15,16,17,18,19].

Enhancing industrialization in the country provides avenue for exporting all exportable products, which is perceived by Osondu [13] as the only way to improve the government revenue, provide export markets for locally produced commodities, products specialization and job creation from export and services in industrial sector. Industrialization greatly depends on production capacity from availability of locally available raw materials used in development of technology in the transformation of the raw materials to finished products [1]. The bases for the development of an industrial sector include access to raw materials, labour force, funds and technology [20]. Availability of raw materials and labour force are not serious problems in Nigeria.

Foundry technology is one of the vital tools for rapid industrial development of any nation [15]. Sand cast is found suitable in casting (foundry technology) of all metals of different sizes, ranging from very small to extremely large sizes [21, 22]. Effective applications of naturally available sand in Nigeria in foundry technology (casting) will help in development of Small and Medium Scale Enterprises (SME). This serves as a good way to solve problem of unemployment, since it has been long believed to be catalysts for economic

growth and national development both in developed and developing countries [23]. According to Safiriyu [24], "Small and medium scale enterprises are strategic to attainment of economic prosperity objective of any government". Adequate utilization of moulding sand as a material foundry processing will help towards enhancement of Nigeria's industrialization. Thus, different locally needed goods and equipment in the country can be robustly produced through indigenous small and medium scale enterprises.

Efficient and economic production of quality sand castings in the modern foundry requires a thorough knowledge of foundry sand technology [25], which can be achieved through testing and analysis of sand properties. This study aims at evaluation of some selected Ado-Ekiti natural moulding sands to desire their suitability for casting applications, by comparing their properties with acceptable materials' standards. Information from this study will at long run assist in boosting the nation's industrialization, positively address problem of unemployment and aid the nation's self-reliance through reduction in importation of foundry sand into the country.

Towards appropriate characterization of the study sands, some of the American Foundry Society's satisfactory mould sand properties for various types of castings were collated from technical literatures is presented in Table 1.

Table 1: American Foundry Society’s Satisfactory Mould Sand Properties for various types of Castings [26,27]

Metal	Clay	Moisture	Green	Dry compressive	Permeability	Flowability
	Content	content	Compressive	Strength	Number	(%)
	(%)	(%)	Strength	(kN/m ²)		
Heavy steel	10-12	4-5	70-85	1000-2000	130-300	-
Light steel	7-12	6-8	70-85	400-1000	125-200	-
Heavy grey steel	10-19	6-8	70-105	50-800	70-120	-
Aluminium	8-10	6.5-8.5	50-70	200-550	10-30	65
Brass and Bronze	10-15	5-7.5	55-85	200-800	15-40	-
Light grey iron	8-13	4-6	50-85	200-550	20-50	-
Malleable iron	8-14	5-7	45-55	210-550	20-60	-
Medium grey iron	11-15	5-8	70-105	350-800	40-50	-

2.0 Materials and Methods

2.1 Materials

The sand samples for this study were collected from four different river banks within Ado-Ekiti metropolis, Ekiti State of Nigeria; situated in between longitude 5⁰ 11' and 5⁰ 25' and latitude 7⁰ 11' and 7⁰ 37'. The river are designated as Sample A (*Omi Amun – Yidi, Poly Road river banks*), Sample B (*Elemi – Housing Road river bank*), Sample C (*Omi Ofin- Iworoko Road river bank*) and Sample D (*Awedele – Textile Road river bank*).

2.2 Methods

2.2.1 Preparation of natural moulding sand

The green sand samples from the above named locations were prepared in

accordance with ASTM and British Standard (BS) Standards [28,29] as discussed in details elsewhere [9]. The samples were then kept in desiccators for further laboratory/experimental analysis,

2.2.3 Production of sand specimens for laboratory analyses

The sand samples for preparation of specimens were prepared and classified for various foundry tests in accordance with the American Foundry-Men Society Standards guidelines [30] as earlier discussed [9,22] to obtain the sands’ foundry properties presented in the results of this study. Some of the specimens produced from the selected natural moulding sands are shown in Figure 1.

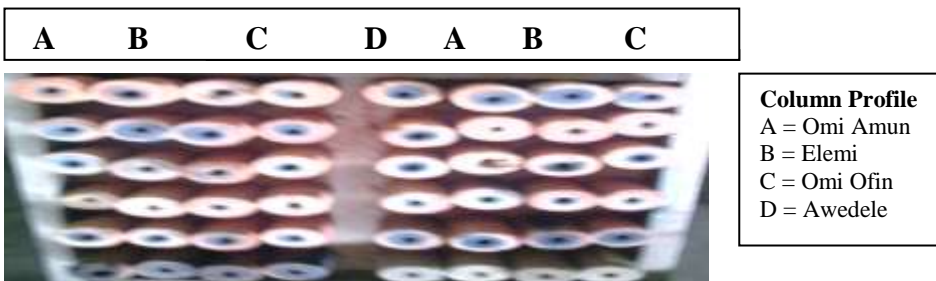


Figure 1: Specimens from the samples of the natural moulding sand

2.2.4 Determination of chemical and physico-mechanical properties of the natural moulding sands

The chemical constituents of the samples of the sand samples were determined using both x-ray fluorescence (XRF) spectrometer and atomic absorption spectrophotometer (AAS). The Physico-mechanical properties of the moulding sands (such as moisture content, clay content, flowability, bulk density, permeability, shatter index, compression strength, green compression strength of natural moulding sand, dry compression

strength, hot compression strength, refractoriness value of moulding sand) were also examined in line with AFS recommendations [30] and the details of the procedures have been adequately discussed elsewhere [9].

4.0 Results and Discussion

Table 2 shows the results of the chemical composition analysis for the selected moulding sands in Ado-Ekiti. The chemical composition of the foundry sand is significant as it relates directly to the metal moulded [31].

Table 2: Chemical Composition of Natural Moulding Sand

Sample	Elemental Composition by Weight (%)									
	SiO ₂	Al ₂ O ₃	CaO	MgO	Na ₂ O	Fe ₂ O ₃	TiO ₂	K ₂ O	MnO	LOI
A	68.35	21.69	0.66	1.37	1.51	2.71	1.67	0.31	0.91	1.23
B	80.59	11.03	3.70	1.54	1.14	0.64	0.23	0.22	0.15	0.76
C	79.98	12.20	0.35	0.40	1.80	1.66	1.11	0.13	1.62	0.75
D	80.29	18.17	0.13	0.23	0.17	0.16	0.11	0.09	0.12	0.53

The percentage of the silica in the moulding sands are within 68.35 and 80.59%, with sample A having the least value (68.35%), while sample B recorded the highest value of 80.59%. The results in Table 2 reveal that the sample sands contain high proportion of silica, which fall within the American

Foundry Society (AFS) standard. According to AFS, most metal casting sand (foundry sand) is high quality silica with physical characteristics [32].

Table 3 presents the results of the selected natural moulding sands' physico-mechanical properties.

Table 3: Some of the properties of the natural moulding sand

Sample	AFS GFN (%)	Clay content (%)	Bulk density (g/cm ³)	Moisture content (%)	Permeability (L/min)	Green strength (kN/m ²)	Dry compression strength (kN/m ²)	Green shatter index (g)	Dry shatter index (g)	Refractoriness (°C)	Flowability (%)
A	63.37	9	12.13	5.71	87.1	83.4	71.5	0.13	0.13	>1200	67.70
B	58.98	12	11.53	6.97	81.9	87.9	93.2	0.33	0.20	>1200	69.00
C	60.238	12	10.93	6.86	82.6	86.5	91.8	0.41	0.30	>1200	68.73
D	51.00	10	11.45	6.11	83.9	85.7	81.7	0.23	0.23	>1200	67.90

The values of the sand samples' AFS-GFN are within the range of 51.00 and 63.37. These values are within 35 to 90, the standard ranges values of fineness number for non-ferrous metal [33] The sand samples tends to have the ability of 2% maximum yields good surface finish at low binder levels; allow low binder level to be used and allows low binder levels, since sand with AFN 50 – 60 with average grain size of 220 – 250 microns and fines content (below 20 microns) has the abilities [34]. This shows that the sands' grain distributions are appropriate for casting since AFS GFN analysis is a useful parameter with the average grain size of the sand with which its choice should be based on particle size distribution [35].

The level of the clay in the sand samples (9 – 13%) is an indication that the natural molding sand is expected to contain sufficient amount of binder material [36], except sample A with 9% clay contents that may require addition of little quantity of binder. The clay content stipulated for moulding sand is between 10 - 12%, while the satisfactory values of clay contents for aluminum, brass and bronze, iron and steel castings are between 12 and 18% [27]. Samples B, C and D with the clay contents between 10 – 12% (Table 3) satisfy the clay content requirements for various metal castings, such as casting of light and heavy steel, heavy grey steel, aluminum, brass and bronze, light grey iron, malleable iron and medium grey iron (Table 1).

Sample A, B, C and D respectively possess bulk density value of 12.13, 11.53, 10.93 and 11.45 g/cm³, which fall within the recommended AFS specification [37]. The recommended bulk density for green moulding sand is 1.49 g/cm³ and above [35].

The percentages of the moisture contents (MC) in the samples as presented in Table 3 are between 5.71 and 6.97%, which are within the satisfactory AFS moulding sand moisture content for various types of castings [33].

Table 3 also shows the permeability values of the sand samples to be between 81.9 and 88.2. An indication that the sand samples possess good natural green permeability for casting a good number of ferrous and non-ferrous metals [27], since their recommended green permeability number for green sand is within 80 – 110. The sand samples green permeability numbers are within the recommended standard ranges. Comparing the samples' permeability numbers with the AFS recommended permeability numbers in Table 1 for casting of various earlier mentioned metals, except heavy and light steel, the values also satisfy the requirements. The sand samples' permeability values reveal the level of well spread grain distribution and rounded-grains of the sand. The permeability depends on grain size, grain shape, grain distribution, binder and its content, degree of ramming and water content of the moulding sand the [14,36,38]. The water content (moisture) of the moulding sand samples has influence on the sand permeability.

Analysis of the results in Table 3 reveals that the high moisture content decreases permeability of the sand. The sand sample (sample A) with highest permeability number of 87.10 also recorded the lowest moisture content (5.71%), while the sand sample (sample B) with the lowest permeability number of 81.90 equally recorded the lowest moisture content (6.97%). Other samples results follow this trend. The

trend of these results is in accordance with assumption that high moisture content (MC) decreases permeability [39]. The samples' moisture contents (5.71 – 6.97%) are found suitable for casting of metals, except for casting of heavy steel (Table 1).

The green compression strength exhibited by Sample A, B, C and D respectively are 83.4, 87.9, 86.5 and 85.7 kN/m². The recommended green sand's strength ranges between 70 and 100 kN/m² [35], while AFS recommends 45 – 105 kN/m² for casting of various categories of metals (Table 1). Each of the sand samples possess adequate green strength that will retain its shape and will not distort or collapse even after the pattern has been removed from the moulding box at moist condition. The strength helps in making and handling the moulds unless the mould is hardened in contact with pattern surface, it will not be possible to achieve dimensional stability and high accuracy of the required size. Compression strength of natural moulding sand is defined as the ability of the sand casting mixture to hold its geometric shape under the conditions of mechanical stress imposed during the sand casting process as the sand's strength [40]. Therefore, the sands' strengths range between 82.0 and 87.9 kN/m².

Also, the values of the dry compression strength exhibited by Sample A, B, C and D respectively are 71.5, 93.2, 91.8 and 81.7 kN/m². This result shows that the dry compression strength increases with the moisture content, in line with the assumption that natural dry compression strength increases with the MC of sand [35]. The sand's strength also depends on the clay and water content, type of clay, the clay size

distribution, among other factors [35]. The moulding sand samples' dry compression strength (71.5 - 93.2 kN/m²) fall within the AFS satisfactory mould sand dry compression strength for casting the various metals, except heavy steel (Table 1).

The experimental results in Table 3 show that the sand sample's strength increases with the moisture content. Moisture content affects the other properties of the mixture such as strength [40]. It was made known that too much moisture can cause steam bubbles to be entrapped in the metal casting. Though, low moisture content in the moulding sand does not develop strength properties [39].

The green and dried shatter index of the specimens ranges between 0.13- 0.41 and 0.13- 0.30 respectively as shown in Table 3. The shatter index values also indicate that the sand samples are tough enough to aid satisfactory lift during pattern withdrawal. The content of clay and corresponding moisture content are attributed to this high value [37].

The refractoriness value of each of the moulding sand sample is above 1200°C (Table 3). A relatively low-uniform thermal linear expansion up to 500°C was observed during the experimental processes. A sudden change in the colour of the specimens to a very reddish colour was also observed at temperature of 600°C. The presence of red oxide in the sands and most of the specimen compressive strengths are in their highest value might be responsible for the sudden change in the colour to reddish. This is an indication that the natural sand in Ado - Ekiti will be suitable for casting of non-ferrous metal of low temperature (like aluminum), as there will be small or no cracks on the mould. The moulding

sand refractoriness must be high to resist high temperature of the molten metal without fuse with metal or breaking down [41].

The specimens' flowability values which are between 67.70 and 67.90% vary in sand with moisture and clay contents [36]. The high flowability value in the sands is as a result of rounded grains nature of the sand. This enhances the ease compaction of the sand [42]. The AFS satisfactory mould sand percentage flowability for casting aluminum is 65 [26, 43, 44, 45]. Flowability increases with decrease in grain size of sand [36].

Conclusion and Recommendation

Conclusion

The following conclusions are drawn from this study:

- i. The sand samples are found to comprise chemical compositions which are within the AFS acceptable limits for moulding sands. The sand samples exhibited high quality of silica suitable as raw sand for low temperature ferrous and nonferrous metal castings, except that of Omi Amun moulding sand sample which has a bit lesser value of silica oxide. This property can be enhanced by

application of additive like bentonite to meet the required limit for most metal casting.

- ii. The results of physico-mechanical properties of the sand samples revealed that studied mould sands' properties are comparable with the standards. Thus, they can be effectively used for adequate casting.
- iii. The physico-mechanical properties of the sand samples also revealed that the sands can be suitably used in casting of metals like grey steel/iron, light steels and aluminum, except heavy steel.
- iv. The presence of red oxide in the sands and most of the specimen compressive strengths are in their highest value show that the natural sand in Ado-Ekiti will be suitable for casting of non-ferrous metal of low temperature.
- v. This study has shown that Ekiti State has potentials of foundry sands and has to take the advantage with suitable conversion technologies.
- vi. The abundant sand resources available are enough for Ekiti to develop the technology of conversion of these resources to usable foundry industries.

References

- [1]. L. N. Chete, J. O. Adeoti, F. M. Adeyinka and O. Ogundele, "Industrial Development and Growth in Nigeria: Lesson and Challenges", Learning to Complete Working Paper No. 8, African Growth Initiative at Brookings Institute /African Development Bank Group / United Nations University UNU-Wider World Institute for Development. Available online: https://www.brookings.edu/wp-content/uploads/2016/07/L2C_WP8_Chete-et-al-1.pdf, Accessed on June 22, 2017.
- [2]. Projectsxta, "Effect of imported goods on Nigeria Economy (Comparative study)". Available online: <http://www.projectsxta.com/resources/302.html>, Accessed on November 3, 2017
- [3]. T. Igberaese, "The Effect of Oil Dependency on Nigeria's Economic Growth". A Master of Arts Research Paper, International Institute of Social

- Studies, The Hague, The Netherlands. Available online: https://thesis.eur.nl/.../ITracy_1_moodledata_temp_turnitintool_793995179._60_1384..., Accessed on November 3, 2017
- [4]. K. Yomi, "Nigeria has now been in recession for five quarters—but there may be light at the end of the tunnel", Quartz Africa, May 23, 2017, Available online: <https://qz.com/989805/nigerias-economy-has-been-in-recession-for-the-fifth-consecutive-quarter/>), Accessed on November 3, 2017
- [5]. Essay UK, "Nigeria's Economy", Available online: <http://www.essay.uk.com/free-essays/economics/nigeria-economy.php>, Accessed on October 13, 2017
- [6]. E. K. Agbaeze, S. N. Udeh and I. O. Onwuka, "Resolving Nigeria's Dependency on Oil – the Derivation Model", Academic Journals, Vol. 7(1), 1-14, 2015.
- [7]. S. Ogege and J. N. Mojekwu, "Trade Policy and the Nigerian Economy- An Econometric Investigation", The Business & Management Review, Vol.3(1), 202-211, 2012.
- [8]. B. A. Udochukwu and I. O. Ogbonnaya, "A Prediction on Nigeria's Oil Depletion Based on Hubbert's Model and the Need for Renewable Energy", International Scholarly Research Network, ISRN Renewable Energy, Vol. 2011, 1-6, 2011, doi:10.5402/2011/285649
- [9]. Y. L. Shuaib-Babata, E. Abegunde and I. O. Ambali, "Evaluation of Chemical and Physico-Mechanical Properties of Ado-Ekiti (South West, Nigeria) Natural Moulding Sands for Foundry Applications, Arid Zone Journal of Engineering, Technology and Environment (AZOJETE) Vol. 13(5), Accepted for publication, 2017.
- [10]. M. Seipati and P. M. Itumeleng, "The Impact of International Trade on Economic Growth in South Africa: An Econometrics Analysis", Mediterranean Journal of Social Sciences, Vol 5 (14), 60-66, 2014. Doi:10.5901/mjss.2014.v5n14p60
- [11]. K. O. Atoyebi, J. O. Akinde, F. O. Adekunjo and E. Femi, "Foreign Trade and Economic Growth in Nigeria: An Empirical Analysis", American Academic & Scholarly Research Journal Vol. 4 (5), Sept 2012, Available online: <http://www.aasrc.org/aasrj>, Accessed on November 3, 2017.
- [12]. B. A. Azeez, S. O. Dada and O. A. Aluko, "Effect of International Trade on Nigerian Economic Growth: The 21st Century Experience", International Journal of Economics, Commerce and Management, Vol. II (10), 1-8, 2014.
- [13]. C. N. Osondu, "Export: Improving Nigerian Government Revenue Base and Economic Diversification", Human Resource Management Research, Vol7(1): 65-73, 2017, DOI: 10.5923/j.hrmr.20170701.08
- [14]. J. O. Aweda and Y. A. Jimoh, "Assessment of Properties of Natural Moulding Sands in Ilorin and Ilesha, Nigeria", USEP: Journal of Research Information

- in Civil Engineering, Vol. 6(2): 68 – 77, 2009.
- [15].Y. L. Shuaib-Babata and J. O. Olumodeji, “Analysis of Ilorin Sand Moulding Properties for Foundry Applications”, International Journal of Engineering Research and Technology (IJERT), Vol. 3(1), 1520 – 1526, 2014.
- [16].B. Adeoye, “Fallacy of Oil Wealth, Resource Curse and Economic Development: Oil Wealth and Income Inequality in Nigeria”, Available online: <https://adeoyebabatola.wordpress.com/2014/02/03/fallacy-of-oil-wealth-resource-curse-and-economic-development/>, Accessed on June 15, 2017.
- [17].F. A. Ovat and M. A. Bisong, “Analysis and Categorization of Akparavini and Okwuboyere Clay Deposits in Biase LGA of Cross River State-Nigeria”, Engineering and Technology. Vol. 4(2):16-21, 2017.
- [18].M. S. Abolarin, O. A. Olugboji and I. C. Ugwuoke , “Determination of Moulding Properties of Locally Available Clays for Casting Operations”. Journal of AU Journal of Technology. 9(4), 238-242, 2006.
- [19].B. K. Isah, “Solid Mineral Resource Development in Sustaining Nigeria’s Economic and Environmental Realities of the 21st Century”, Journal of Sustainable Development in Africa, 13 (2), 210-214, 2011.
- [20].J. R. T. Hughes, “Industrialization. International Encyclopedia of the Social Sciences, Thompson Gale, Canada”, Available online: <http://www.encyclopedia.com/history/united-states-and-canada/us-history/industrialization#B>, Accessed on July 12, 2017.
- [21].Web I. Available from http://thelibraryofmanufacturing.com/metalcasting_sand.html, Accessed on 22 February, 2017.
- [22].Y. L. Shuaib-Babata, A. J. Abegunde and J. M. Abdul, “Suitability of Ado-Ekiti (Nigeria) Natural Moulding Sands for Use as Foundry Sands in Aluminum Alloy Casting”, Journal of Production Engineering, Vol. 20(2), 2017 (Accepted for publication).
- [23].F. Abiodun, “Small and Medium Scale Enterprises in Nigeria: The Problems and Prospects”, Department of Political Science, Faculty of Social Sciences, Lagos State University, Ojo, Lagos, Nigeria, Available online: www.academia.edu/1406990/SMALL_AND_MEDIUM_SCALE.., Accessed October 18, 2017.
- [24].A. M. Safiriyu, “Impact of Small and Medium Scale Enterprises in the Generation of Employment in Lagos State”, Kuwait Chapter of Arabian Journal of Business and Management Review Vol. 1 (11), 109 -141, 2012.
- [25].F.L. Le Serve, “Sands and Sand Preparation”, In: Beadle J.D. (eds) Castings. Production Engineering Series. Palgrave, London, 1971, https://doi.org/10.1007/978-1-349-01179-7_5,
- [26]. A. M. Mikhailov, “Metal Casting”, Mir Publishers, Moscow, pp 71-82, 1989.
- [27]. T. A. Burns (Eds), “Foseco Ferrous Foundryman’s Handbook”. Butterworth

- Heinemann., New Delhi, India, pp. 1- 352, 1989.
- [28]. K. H. Head, “Manual of Soil Laboratory Testing: Soil Classification and Compaction Tests”, Volm 1, Fentech Press, Plymouth, London, pp 1-388, 1997.
- [29]. K. H. Head, “Manual of Soil Laboratory Testing: Permeability, Shear Strength and Compressibility Tests”, Vol. 2, Fentech Press, Plymouth, London, pp 1-747, 1997.
- [30]. American Foundry-Men Society Standards (AFS), “Mould and Core Testing Handbook”, 2nd ed, Foseco Ltd, Pergamon Press, Oxford, England, pp. 113, 1982.
- [31]. J. O. Akinyele and K. S. Oyeyemi, “Strength Behaviour of Concrete using Foundry Sand as Aggregate”, Journal of Natural Science, Engineering and Technology, Vol. 13: 99-108, 2014.
- [32]. American Foundry Society (AFS), “Introduction to Foundry Sand”, Available online:<http://www.afsinc.org/content.cfm?ItemNumber=7075>, Accessed on October 28, 2017
- [33]. T. A. Burns, “Foseco Foundry man’s Handbook”, 9th ed, Foseco (F.S.) Ltd., Tamworth Staffordshire, Pergamon Press, Oxford, England, pp. 435, 1986.
- [34]. B. E. Tuncer, “Foundry Sand: Characteristics, Specifications, Environmental Considerations, Availability”, Recycled Materials Resource Center (RMRC), University of Wisconsin-Madison, pp 1-7, 2017.
- [35]. A. P. Ihom, J. Agunsoye, E. E. Anbua and J. Ogbodo, “Effects of Moisture Con on the Foundry Properties of Yola Natural Sand”, Leonardo Electronic Journal of Practices and Technologies, Vol. 9, 85-96, 2011.
- [36]. ME Mechanical, “Molding Sand: Constituents, Types and Properties”, Available online: <https://me-mechanicalengineering.com/molding-sand/>, Accessed on December 7, 2016.
- [37]. A. Tokan, E. A. Adelemoni and S. G. Datau, “Mould Characteristics of Azare Foundry Sand”, Journal of Raw Material Research (JORMAR), Vol. 1(1), 67-78, 2004.
- [38]. Web II, Available on line: <http://www.iitbhu.ac.in/faculty/min/rajesh-rai/NMEICT-Slope/lecture/c6/13.html>), Accessed on October 17, 2017.
- [39]. Mechanical Engineering, “A complete online guide for every Mechanical Engineer-Sand testing methods sand testing equipment”, Available online: <http://www.mechanicalengineerin-gblog.com/2997-sand-testing-methods-sand-testing-equipment/>, Accessed on December 7, 2016.
- [40]. Sand Casting (2017). Available online: http://thelibraryofmanufacturing.com/metalcasting_sand.html, Accessed on January 22, 2017.
- [41]. S. A. Ibitoye, J. O. Olawale and M. D. Shittu, “Influence of Cement-Silica Ratio on the Moulding Properties of Portland Cement Bonded Sand”, Journal of Physical Science, Vol. 25(1), 113–122, 2014.
- [42]. Casting and Welding, Lecture Notes on Advanced Casting and

- welding (ACW), SSM College of Engineering and Technology, Department of Mechanical Engineering. Available online: <https://ssmengg.edu.in/weos/weos/upload/EStudyMaterial/Mechanical/4thSem/production-technology/CastingAndWelding.pdf>, Accessed on 25 May, 2017.
- [43] H. W. Dielert, "Foundry Core Practice". American Foundry Men's Society. 3rd ed., Des Plaines, 1966.
- [44]. R. B. John, "Foseco Ferrous Foundry Man's Handbook", Replica Press Ltd., India. pp 256, 2000.
- [45]. N. A. Ademoh and A. T. Abdullah, "Assessment of Foundry Properties of Steel Casting Sand Moulds Bonded with the Grade 4 Nigeria Acadia Species (Gum Arabic)", International Journal of Physical Sciences, Vol. 4(4), 238-241, 2009.



Development of an Encrypting System for an Image Viewer based on Hill Cipher Algorithm

**Okereke Chinonso, Osemwegie Omoruyi,
Kennedy Okokpujie & Samuel John**

Department of Electrical and Information Engineering,
Covenant University,
Ota, Ogun state, Nigeria

Corresponding Author: Kennedy.okokpujie@covenantuniversity.edu.ng

Abstract: Security breaches to personal computing devices, cloud storage accounts, portable media devices are rampant in today's world. Also, Increased intrusions into corporate servers and employee workstations often times lead to the unwarranted exposure of an individual or corporate secret and a breach to privacy. Information leaked through such intrusions and breaches especially images are often times in the public terrain without a user's or corporate consent. This breaches are due to a variety of reasons including internal saboteurs, theft, social engineering or a computer security attack. At times other crimes like fraud, blackmail, kidnapping and assassinations may follow. This study presents the development of an Encryption system in an Image Viewer Application. Encrypting Images before storage or transfer to any platform helps limit risk when images are stolen or leaked. The image viewer was designed in C#.NET using the Hill Cipher algorithm for Image Encryption and Decryption. The results for images are shown to be good for two image samples. However, low key image samples produce a better result after Encryption. In general, Encryption of user generated images is a vital security strategy and a good option to have to prevent against a growing number of threats.

Keywords: Images, Pictures, Cryptography, Encryption, Information Security, Cipher, Viewer.

1.0 Introduction

Pictures speak louder than words, so says a popular English proverb. Images have the ability to communicate non-verbally to people of all races or colour excepting the visually impaired or challenged. The surge in social media's popularity is in no small way down to amongst many factors the use of diverse media especially images in varying formats used in communicating individual opinions and views [1]. Images are also vital to individuals, corporations and brands because they can communicate a variety of emotions including excitement, scorn, anger, embarrassment and humour. In 2013, Facebook, the world's largest social media base, noted on average that 350 million images are uploaded to its platform daily, an estimated 4000 images per second [2, 3].

There has also been a steady increase in Cloud storage i.e. Storage as a service platforms as an alternative to traditional user owned storage media (Flash drives, Compact Disc, External Hard drives, System Hard Drives). Computing and Mobile devices now carry software applications that make movement of images to such platforms seamless and easy. This has also encouraged a commensurate increase in user generated imagery and pictures. New platforms have also arisen from related to the Cloud storage trend, a good example user generated news platforms hosted by Electronic and Print Media for harvesting news contents. By using cloud storage such platforms support the upload of news stories using Images and Visuals. Although all of this can be judged as a positive trend, there are also the accompanying security risks and threats heralded by such developments. Breach to the security of private user generated images on web, social media, cloud storage and portable device

platforms are on the increase. Such vulnerabilities on this respective platforms highlighted have become tools for nefarious actors to carry out non-technical attacks like social engineering and to perpetrate other crimes like fraud, blackmail, human trafficking, kidnapping and assassinations. Several of this platforms have responded by tightening privacy controls especially on web platforms, restricting users who can view particular information like images. However, they are not adequate to cover all risks posed by users on such platforms. A preventive strategy on the rise is that of encrypting information communicated between users but there are also legal and juridical challenges to this approach. Encryption of information employs specialised techniques of ciphering user content so that only legitimate or proper recipients are able to decipher such information with the aid of a special key. Adoption of encryption needs to be more prevalent on many platforms to limit and mitigate risks posed to users on a variety of platforms where image dissemination, transfer or storage is done.

This study details the development of an Encryption system in an Image Viewer Application for a variety of Image formats that uses the Hill Cipher cryptographic algorithm for encrypting viewed images on the go. Users also have the option of decrypting the Images for private viewing. The studies outline is as follows: Section 2 explains the Hill Cipher Algorithm. Section 3 covers the design phase of the developed encryption system. Section 4 outlines the results achieved for various Images. Section 5 concludes the study.

2.0 Review of Hill Cipher Algorithm

Hill Cipher was developed in the late 1920s by Lester Hill [4, 5]. The Hill cipher is a polygraphic substitution cipher [6] where a block of at least two numbers are replaced with another block of numbers or symbols with the same size. This mix is done using matrices and matrix manipulations. The Hill Cipher has several advantages including defending against attack by frequency analysis of cipher values [7, 8]. Hill Cipher also is very advantageous in data and plaintext encryption [4]. Implementation of the Hill Cipher requires linear algebra and modulo arithmetic. The ideal algorithm is a symmetric key algorithm where the same key (which could be a self-invertible key) for encryption is used also for decryption of a set of values. However, a regular invertible key would have to be inverted if it's to be used for decryption.

A matrix is said to be invertible if $M \cdot M^{-1} = I$, where M^{-1} is the inverse of M and I is an identity matrix. In the case of the hill cipher key k , $K \cdot K^{-1} = I$ is the requirement for an application generated or used encryption key. It is obvious that for a matrix to be invertible it must be a square matrix but it is also true that not all square matrices are invertible. A matrix is not invertible if its determinant equals zero. A simple example is a matrix $B = \begin{pmatrix} 2 & 2 \\ 1 & 1 \end{pmatrix}$, where the determinant is $2 \times 1 - 2 \times 1 = 0$ and the resultant inverse $\frac{1}{0}$ is undefined. This is said to be a singular matrix.

Digital Images can be modelled as a three band monochrome image data [9], i.e. Red-Green-Blue (RGB) components, each component been an 8 bit value ranging from 0 - 255 in

decimal or 00- FF in hexadecimal. Discarding the Alpha component of our images, a three pixel bitmap block P

contains $\begin{pmatrix} R_1 \\ R_2 \\ R_3 \end{pmatrix}$, $\begin{pmatrix} B_1 \\ B_2 \\ B_3 \end{pmatrix}$ and $\begin{pmatrix} G_1 \\ G_2 \\ G_3 \end{pmatrix}$ and

requires a key

$$K = \begin{pmatrix} K_{11} & K_{12} & K_{13} \\ K_{21} & K_{22} & K_{23} \\ K_{31} & K_{32} & K_{33} \end{pmatrix} \text{ for encryption}$$

to get the cypher image component:

$$C = \begin{pmatrix} RC_1 \\ RC_2 \\ RC_3 \end{pmatrix}, \begin{pmatrix} BC_1 \\ BC_2 \\ BC_3 \end{pmatrix} \text{ and } \begin{pmatrix} GC_1 \\ GC_2 \\ GC_3 \end{pmatrix}.$$

More clearly,

$$\begin{pmatrix} RC_1 \\ RC_2 \\ RC_3 \end{pmatrix} = \begin{pmatrix} K_{11} & K_{12} & K_{13} \\ K_{21} & K_{22} & K_{23} \\ K_{31} & K_{32} & K_{33} \end{pmatrix} \begin{pmatrix} R_1 \\ R_2 \\ R_3 \end{pmatrix} \text{ mod } 256$$

$$\begin{pmatrix} BC_1 \\ BC_2 \\ BC_3 \end{pmatrix} = \begin{pmatrix} K_{11} & K_{12} & K_{13} \\ K_{21} & K_{22} & K_{23} \\ K_{31} & K_{32} & K_{33} \end{pmatrix} \begin{pmatrix} B_1 \\ B_2 \\ B_3 \end{pmatrix} \text{ mod } 256$$

$$\begin{pmatrix} GC_1 \\ GC_2 \\ GC_3 \end{pmatrix} = \begin{pmatrix} K_{11} & K_{12} & K_{13} \\ K_{21} & K_{22} & K_{23} \\ K_{31} & K_{32} & K_{33} \end{pmatrix} \begin{pmatrix} G_1 \\ G_2 \\ G_3 \end{pmatrix} \text{ mod } 256$$

$$RC_1 = (K_{11}R_1 + K_{12}R_2 + K_{13}R_3) \text{ mod } 256$$

$$RC_2 = (K_{21}R_1 + K_{22}R_2 + K_{23}R_3) \text{ mod } 256$$

$$RC_3 = (K_{31}R_1 + K_{32}R_2 + K_{33}R_3) \text{ mod } 256$$

$$\text{or } RC = KR.$$

For decryption to retrieve the original decomposed RGB components, $R = K^{-1} \cdot RC$. For the encryption key to be the same as the decryption key, Hill Cipher requires that the key k be a self-invertible matrix. In this case, $M = M^{-1}$. Panigrahy et al [4] expounds on solving and obtaining self-invertible matrices in detail. Using a self-invertible key may lengthen

computation time because matrices would have to be generated and tested using the self-invertible condition.

3.0 Design of the Crypto Viewer

Based on the Hill Cipher algorithm, the Crypto viewer design flowchart shows the various sequence of steps and iterations in carrying out the encryption of an image divided into two stages.

The first stage, involves the splitting of the image into Red-Green-Blue (RGB) components. The components are stored as separate arrays (R_{array} , G_{array} and B_{array}). The Alpha components although important is not used in this study. Alpha component contains details on image luminance.

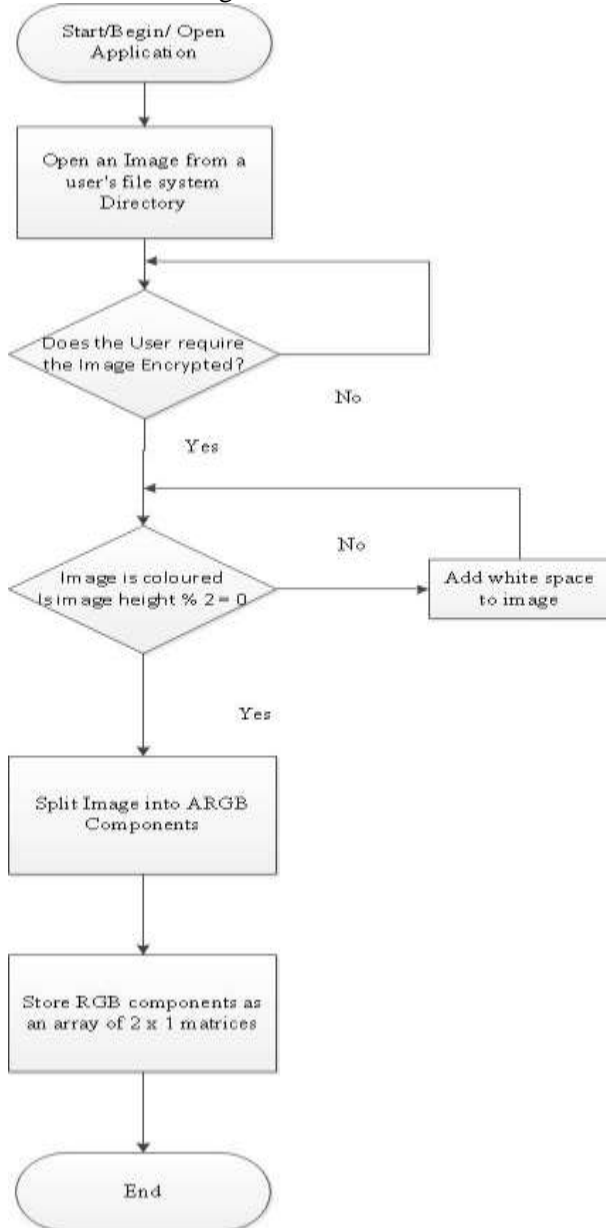


Figure 1. Decomposing of Image into RGB components

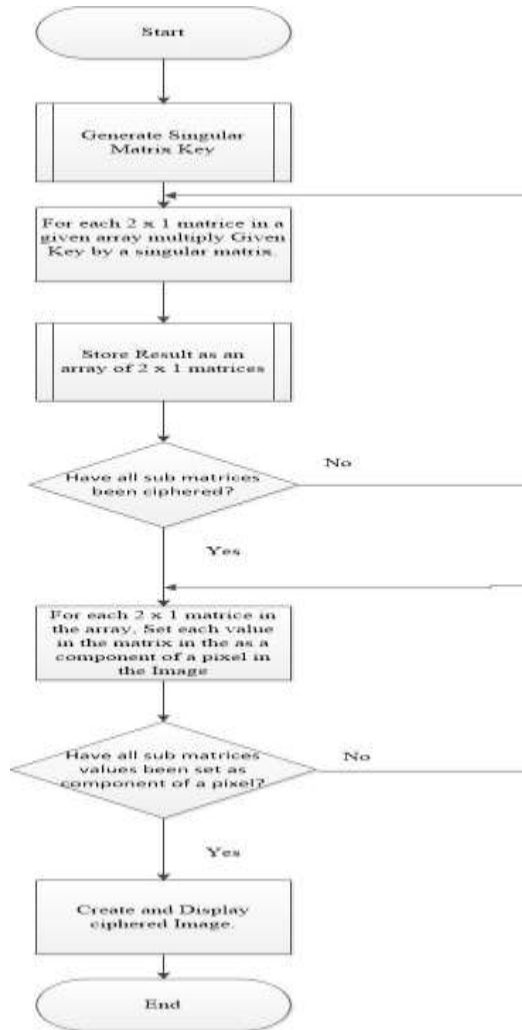


Figure 2. Generation of Encryption Key and the creation of an Encrypted Image.

4.0 Implementation

The results from two images are displayed as seen from Figures 3a, 3b, 3c, 4a, 4b and 4c. High value (key) images are a lot more recognizable after encryption. Low value (key) images i.e. images with more pixels closer to full

amplitude produce better results on the whole. The processing speed of large images i.e. Images larger than 100KB takes > 15 seconds as seen in Table 1. Image formats can be .jpg .png, .jpg, .bmp or .gif.



Figure 3a. Original high key image

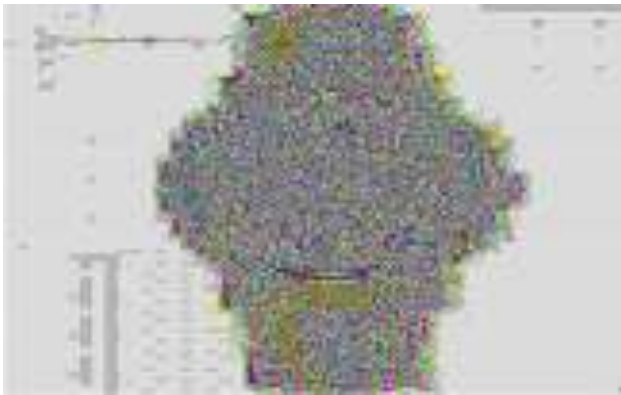


Figure 3b. Encrypted high key image



Figure 3c. Decrypted image result



Figure 4a Original low-key Image



Figure 4b Encrypted low-key image



Figure 4c Decrypted image result

System Information	Intel Pentium B960 2.20 GHz 4GB memory		
Image name	Encryption time(s)	Format	Size in KB(resolution)
Watch	2..2657	.jpg	18.1(400 x 400)
Old Custom Office	16.125	.jpg	143.0(1280 x 1116)

Table 1: System specification and Image Information

5.0 Conclusion

The unpredictability of an encryption scheme is always a desirable trait of any encryption tool. The above viewer makes the encryption of images fast for any user. However, more security could mean that tool can make use of a random key sizes whilst key size length and key could be stored as Meta data also in Encrypted format with the images. The encryption scheme can also be randomly chosen such that encrypted image results are more difficult to retrieve. Encrypted Images in this case are of a hybrid form. Image

RGB components can also be randomly stored in key value stores and served on the fly for web based applications aside from a device based scenario.

Acknowledgements

We acknowledge the support of Covenant University in conducting this research and the cost of publication.

Further Study

This study hopes to further evaluate using a variety of encryption quality metrics the effectiveness of the hill cipher algorithm for image encryption.



Figure 5: Image Viewer Interface

References

- [1] A. Lenhart, K. Purcell, A. Smith, and K. Zickuhr, "Social Media & Mobile Internet Use among Teens and Young Adults. Millennials.," Pew Internet Am. Life Proj., pp. 1–37, 2010.
- [2] B. Thomee et al., "YFCC100M: The New Data in Multimedia Research," 2015.
- [3] "Facebook by the Numbers (2017): Stats, Demographics & Fun Facts." [Online]. Available: <https://www.omnicoreagency.com/facebook-statistics/>. [Accessed: 14-Oct-2017].
- [4] S. K. Panigrahy, B. Acharya, and D. Jena, "Image Encryption Using Self-Invertible Key Matrix of Hill Cipher Algorithm," Image (Rochester, N.Y.), no. February, pp. 21–22, 2008.
- [5] K. Mani and M. Viswambari, "Generation of Key Matrix for Hill Cipher using Magic Rectangle," vol. 10, no. 5, pp. 1081–1090, 2017.
- [6] B. Acharya, S. K. Patra, and G. Panda, "Involuntary, Permuted and Reiterative Key Matrix Generation Methods for Hill Cipher System," Int. J. Recent Trends Eng. Vol. 1, No. 4, May 2009, vol. 1, no. 4, pp. 106–108, 2009.
- [7] M. Mokhtari, "Analysis and Design of Affine and Hill Cipher," vol. 4, no. 1, pp. 67–77, 2012.
- [8] Chris Christensen, "Introduction to Hill cipher," Lecture note. [Online]. Available: <https://www.nku.edu/~christensen/092mat483/hill/cipher.pdf>. [Accessed: 30-Sep-2017].
- [9] S. E. Umbaugh, Computer Imaging: digital image analysis and processing. CRC press, 2005.



Evaluation of Blends of Agricultural Solid Biomass Waste for Solid Fuel Production

**Augustine O. Ayeni*, David O. Odede, Ayodeji Ayoola,
Opeyemi Adeayo & Ajibola Ogunbiyi**

Department of Chemical Engineering,
Covenant University, Canaanland, Ota, Nigeria
*augustine.ayeni@covenantuniversity.edu.ng;
aoayeni@gmail.com

Abstract: In this study, the calorific values of solid fuel samples and their blends in different proportions were determined. Waste samples as sawdust, charcoal, palm kernel bagasse, palm kernel shell, corn cob, palm fronds and coconut shell were subjected to combustion in an isothermal bomb calorimeter and their heating temperature profiles and corresponding heating values were estimated. Individual materials and different blending ratios in weight by weight (1:1, 1:1:1, 3:1:1, 1:3:1, and 1:1:3) heating contents were established. Burning time test was evaluated for blended materials with highest caloric values. Charcoal had the highest calorific value amongst all individual samples with a calorific value of 17,062 kJ/kg with palm fronds having the least heating value of 12,997 kJ/kg. In the 1:1 ratio mix, charcoal:palm oil bagasse had the highest heating content of 21,907 kJ/kg. Considering the ratios of three different solid mass in varying weight proportions, the combination of charcoal:coconut shell:palm oil bagasse (1:1:1) in equal weight percent gave the highest heating content of 23,373 kJ/kg. The blend of charcoal:coconut shell:palm kernel bagasse had the highest burning time of 20 minutes and 12 seconds. From the evaluations, charcoal in mixed proportions with other solid biomass are excellent materials to be considered for solid fuels production.

Key Words: Biomass; Bomb calorimeter; Caloric value; Combustion; Pellets

1. Introduction

Energy security, global warming and proper use of locally sourced materials are the driving factors for using biomass as an alternative energy source [1]. Biomass fuel utilization provides great advantages for the environment. Biomass absorbs carbon dioxide during growth, and emits it during combustion. As a result, biomass helps the atmospheric carbon dioxide recycling, does not contribute to the greenhouse effect, and consumes some amount of CO₂ from the atmosphere during growth and releases the same during combustion [2]. Fossil fuel, a non-renewable form of energy, provides 80 percent of man's energy [3]. This conventional form of energy is being gradually depleted through the growing world industrialization. In addition, the utilization of fossil fuel for industrialization has negative effects on the world's climatic conditions such as the emission of greenhouse gases into the atmosphere leading to global warming. Increasing industrial activities and world's population are related to the general energy utilization. It is estimated that world's energy demand will be more than 50% by 2025 [4]. A good solution to reducing all these setbacks brought about by the utilization of fossil fuel for world's industrial development is to investigate and to find new alternative fuel sources. Biomass is said to be the third largest energy resource in the world after coal, gas and oil [5].

Biomass is nearly carbon neutral; hence its utilization helps mitigate greenhouse gas emissions [1]. Use of traditional biomass fuels in combustion systems, either alone or in combination with oil or coal, reduce emissions of NO_x, SO₂ and CO₂ compared to using fossil fuels alone [6]. Waste materials from sawdust, papers, leaves, rice husk,

coconut husks, corn cob, palm kernels, palm oil bagasse, and other agricultural wastes in many combinations and proportions can be developed into fuel briquettes or pellets [7], [8]. Many of these agricultural materials lie as waste heaps not utilized adequately. In such waste dumps, these materials get decayed ultimately releasing carbon dioxide to the atmosphere. These materials could be used to produce pellets or briquettes which are a form of fuel. Biomass pellets are usually in form of cylindrical sticks. They are utilized in home pellet stoves, central heating boiler, industrial boiler, or in power plants. Biomass briquettes can be in form of sticks or blocks with large diameter and different shapes. They are primarily for industrial use for heating. Briquette making has the potential to meet the additional energy demands of urban and industrial sectors, thereby making a significant contribution to the economic advancement of any country. Due to high moisture content, irregular shape and size, and low bulk density, biomass is very difficult to handle, transport, store, and utilize in its original form [9]. As a result of these setbacks, densification of these materials into durable compact forms (as pellets or briquettes) is effective in solving these challenges and can reduce material waste. Densification can increase the bulk density of biomass from an initial bulk density of 40-200 kg/m³ to a final compact density of 600-1200 kg/m³ [10], [11]. Also, densified biomass, as pellets, has drawn attention due to its superiority over raw biomass in terms of its physical and combustion characteristics [12]. The utilization of these biomass materials also depends on the following: feed constituents, energy content, volatile matter, ash content and slagging characteristics, reactivity, size and size

distribution, adding binders or additives, densification equipment, bulk density, and post- production treatment conditions like heating or cooling and storage conditions [13]. These properties could be altered by subjecting raw biomass to various processing methods and forming composites [11]. If biomass or agro-waste briquettes are to be used efficiently and rationally as fuel, they must be characterized to determine parameters such as the calorific values, flame propagation rates, ignition time, burning time, burning efficiency among others. The calorific (heating) value of biomass feed-stocks are indicative of the energy they possess as potential fuels. The gross calorific value (higher heating value, HHV) and the net calorific value (lower heating value, LHV) at constant pressure measures the enthalpy change of combustion with and without water condensed, respectively [14]. Most agricultural wastes as those considered in this study can be converted from solid to either gaseous or liquid fuels by biochemical, thermal and chemical processes [15]. Adequate utilization of biomass fuels gives enormous benefits in terms of environmental concerns. During their growth, biomass absorbs carbon dioxide during growth, and emits it during combustion. In addition, biomass as fuel for power production offers the advantage of a renewable and CO₂-neutral fuel [2].

In this study, the energy contents of some agricultural solid wastes and their mixed proportions were investigated amenable to further large-scale pelletising or briquetting. Variations of energy contents based on samples mixing ratios, burning time, ignition and ashing time were evaluated.

Furthermore, the best combination of these variations was established.

2. Materials and Methods

2.1. Materials Sourcing and Preparation

Charcoal was collected at a local cooking store while sawdust was sourced from a wood milling factory, both at Ikorodu Town (6o37'N 3o30'E, elevation of 28 m), South West, Nigeria. Coconut shell, corn cob, palm fronds, palm oil bagasse, palm kernel shell were all sourced from a farm settlement at Iju Town (7o22'N 5o15'E, elevation of 353 m), South West, Nigeria. Samples were sun dried for approximately 48 hours to reduce their moisture contents. All samples were pulverized to accepted size fractions. Samples were made to pass through sieves of different aperture diameter ranging from 500 μ m to 106 μ m. The samples were further dried in a convection oven at 105 oC to completely eliminate moisture. The dried materials were stored in different rubber packs until they were ready to be used.

2.2 Determination of Heat of Combustion of Materials

The heating value measurement or the heat of combustion of the individual raw materials and their mixed proportions were determined by an isothermal oxygen bomb calorimeter (Fig. 1). The bomb calorimeter consists of metal bomb designed to withstand heat and pressure, a large flask to hold the bomb and a known volume of water, which are means of remotely igniting the sample (typically electrically, through the use of a fuse wire), and a means of accurately measuring the temperature of the water. The heating or calorific value of a fuel sample is the amount of heat liberated

per unit mass of the sample. After standardization with benzoic acid (standard heating value of benzoic acid was determined and its known heat of combustion was used to determine the heat capacity of the bomb calorimeter). Once the calorimeter has been calibrated, the caloric values of raw samples were determined. 1.0 g of grounded sample (150 μm size fraction) was weighed and pelletized using the pellet press (Fig. 2(a)). The pelletized material was burnt in the bomb calorimeter for a particular duration. For each batch of experiments, 0.1 m of chromium wire was attached to the bomb electrodes. The wire was bent so that the loop bears against the top of the pellet firmly enough to keep it from sliding against the side of the capsule. The bomb was placed securely on the bomb basket after injecting oxygen at 2,020 kPa into the bomb through the knurled valve knob. 2 L of distilled water was poured into the metal bucket sufficient to submerge the nut of the bomb to a depth of 0.003 m (Fig. 2(b)). An initial 10 min was allowed before the firing temperature was noted. After the initial temperature rise and with no reasonable change in temperature, the bomb was removed from the calorimeter, and residual gas was allowed out of the bomb by opening the knurled valve knob. The remaining length of the fuse wire was recorded in order to determine the correction for firing energy. Oxygen was supplied to the bomb calorimeter before immersion into the bucket with compressed oxygen present in a gas cylinder at 20

atmospheres. Acid correction is carried out after each step to correct for any incomplete combustion in the calorimeter using 0.1 M sodium hydroxide solution. All measurements were duplicated. The schematic diagram of the isothermal bomb calorimeter is as shown in Fig. 1.

A resultant energy value for any material tested was calculated from;

$$Q_v = \frac{E (\Delta T - C_1 - C_2)}{M_{ST}}$$

Q_v = Caloric value of sample at the final temperature (kJ/kg)

M_{ST} = Weight of the standard sample

C_1 = Correction for firing energy (determined from the left over of the chromium wire burning equal to 2.6 x length of chromium burnt)

C_2 = Total acid correction (determined from the after-wash solution of the interior of the bomb by titrating with 0.1 M NaOH solution)

ΔT = Measured change in temperature

E = Energy equivalent of the bomb calorimeter (J/degree ($^{\circ}\text{C}$)), given as;

$$E = \frac{Q_{ST}(M_{ST} + C_1 + C_2)}{\Delta T}$$

Q_{ST} = Heat of combustion of the standard sample (benzoic acid)

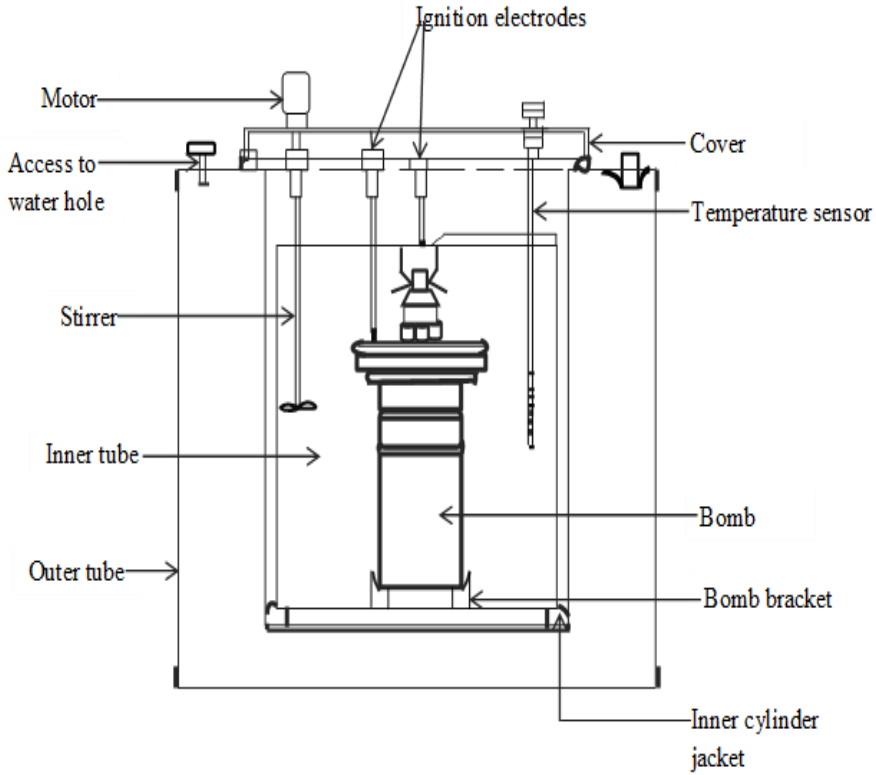


Fig. 1. Schematic representation of a simple isothermal oxygen bomb calorimeter



Fig. 2. (a) and (b) views of manual pelletizing set up and calorimetric bomb immersed in the metal bucket respectively.

Materials in mixed proportions were bound with starch paste, mould into small shapes and sun dried. The mixed proportions were investigated as blends of materials in 1:1 ratio (using either sawdust or charcoal in same proportions

with the other materials) and combining the best three materials that gave the highest individual heating contents in four different ratios (Table 1). The burning time was

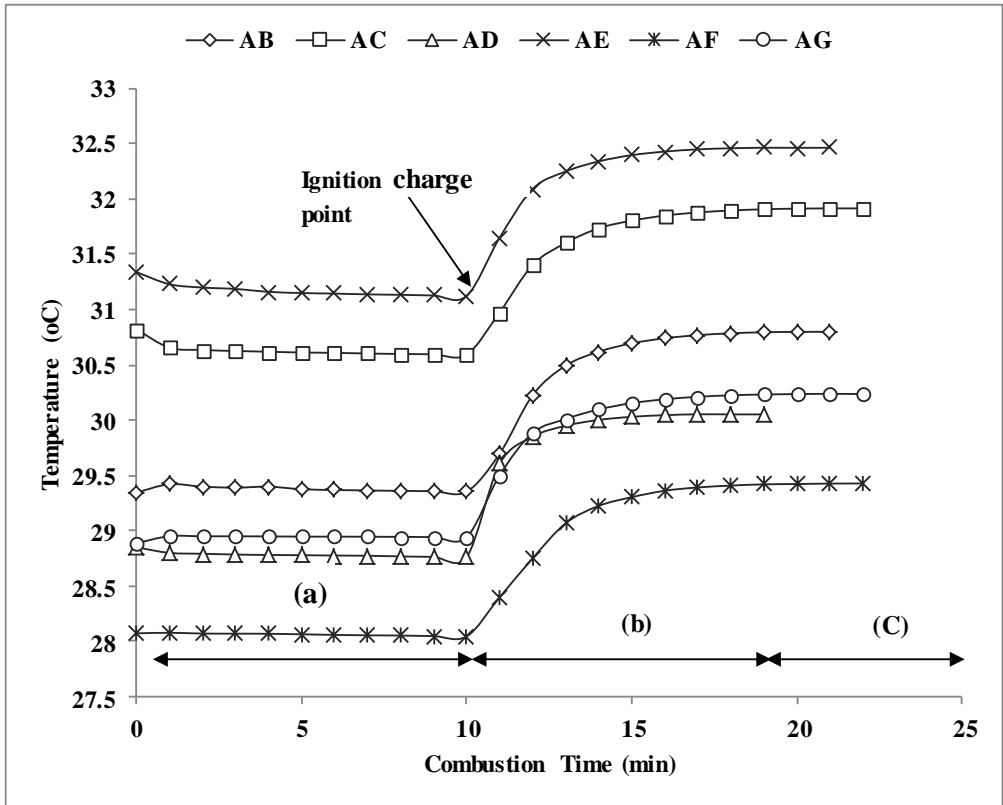


Fig. 3. Temperature profile illustration during the combustion of blends of charcoal with other materials in 1:1 mixed proportions (B = Coconut shell, C = Corn cob, D = Palm fronds, E =

Palm oil bagasse, F= Palm kernel shell, G= Sawdust). Section (a) is the initial temperature test period, section (b) is the temperature rise period, and section (c) is the final temperature test period.

Table 1: Estimated Heating Values of Individual Materials and their Mixed Proportions.

Sample	Heating content (kJ/kg)	Mixed proportion (1:1)			
		Sample	Heating content (kJ/kg)	Sample	Heating content (kJ/kg)
A (Charcoal)	17,062	AB	21,299	GA	19,219
B (Coconut shell)	16,480	AC	20,337	GB	16,681
C (Corn cob)	10,798	AD	17,325	GC	15,270
D (Palm fronds)	12,997	AE	21,907	GD	14,820
E (Palm oil bagasse)	16,307	AF	19,890	GE	15,744
F (Palm kernel shell)	15,396	AG	19,219	GF	15,908
G (Sawdust)	14,941				
Mixed proportions Heating content (kJ/kg)	A:B:E 23,373	A:B:3E 18,598	3A:B:E 21,891	A:3B:E 18,740	

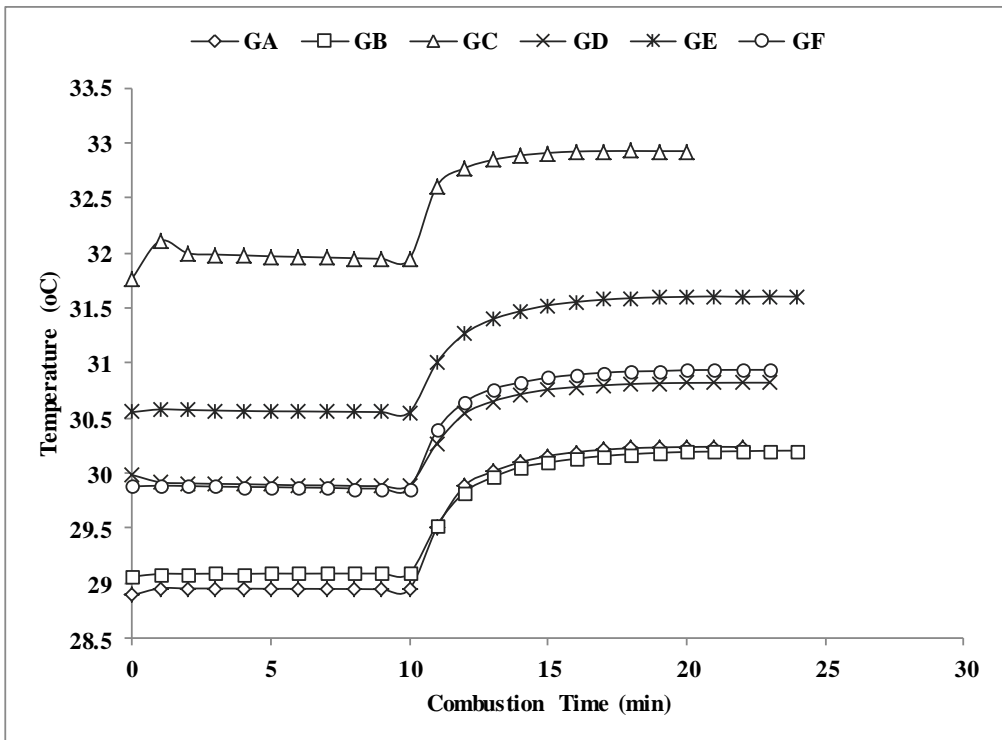


Fig. 4. Temperature profile illustration during the combustion of blends of sawdust with other materials in 1:1

mixed proportions (A = Charcoal, B = Coconut shell, C = Corn cob, D =Palm fronds, E= Palm oil bagasse, F= Palm

kernel shell). taken as the difference between ignition time and ashing time (time of samples completely turning to ash) of different mixed samples.

3. Results and Discussion

3.1 Heating Contents of Individual and Blended Materials

The measured temperatures for the different blends of materials in different mixes (using charcoal and sawdust as the materials with highest individual energy contents) are given in Fig. 3 and Fig. 4. The caloric values for individual materials were obtained in kJ/kg as (Table 1); charcoal (17,062), coconut shell (16,480), corn cob (10,798), palm fronds (12,997), palm oil bagasse (16,307), palm kernel shell (15,396), sawdust (14,941). Corn cob has the least heating content. In a previous study [6], the caloric value of plain sawdust briquette was obtained as 18.82 MJ/kg. This value is greater than the caloric content of raw sawdust in this study. This may be due to variations in the species and experimental conditions. The caloric value of charcoal is the highest among the individual heating contents. The firing temperatures of blended materials (at zero time) corresponding to a particular temperature increases with the burning strengths of the materials (Fig. 3 and Table 1). For example, AB (charcoal: coconut shell; 21,299 kJ/kg) has temperature of 29.4 oC. In addition, AE (charcoal: palm oil bagasse; 21,907 kJ/kg) has temperature of 31.4 oC. Equally, for the 1:1 mixed proportions of sawdust with other materials, GA (sawdust: charcoal) produced the highest heating content of 19,219 kJ/kg

References

- [1] A. Sultana, A. Kumar, and D. Harfield, "Development of agri-pellet production cost and

with the highest firing temperature of 31.7 oC.

3.2 Burning and Ashing rates of Blended Materials

Generally, solid fuel samples ignite easily due to the presence of large amount of inorganic salts. In this study, the blend of charcoal, palm kernel shell and coconut shell in ratio 3:1:1 respectively ignited very fast at 1 minutes and 30 seconds. This was as result of the large proportion of charcoal which is very rich in carbon. The presence of charcoal in a blend makes the blend easily fireable. The blend also had a long burning time making a good fuel source.

4. Conclusions

The choice of a biomass for energy conversion will in part be decided by its heating value. All solid mass pellets examined in this study had no problem in the combustion procedure. The heating contents of all materials tested varied from the lowest at 10,798 kJ/kg (corn cob) to the highest in a mixed proportion of 1:1:1 (charcoal, coconut shell, and palm oil bagasse) having heating value of 23,373 kJ/kg. The presence of charcoal in any form of solid fuel blend increases the calorific value of such blend. Palm kernel bagasse had a higher calorific value than palm kernel shell because of the presence of combustible fibers in palm kernel bagasse. Amongst the individual samples investigated, charcoal had the highest calorific value of 17,062 kJ/kg with palm fronds having the least heating value of 12,997 kJ/kg. Charcoal and its blends had the highest burning rates.

optimum size," Bioresour. Technol., vol. 101, pp. 5609-5621, 2010.

- [2] A. Demirbas, Combustion characteristics of different biomass fuels, "Prog. Energy Combust. Sci.," vol. 30, pp. 219-230, 2004.
- [3] R. E. H. Sims, R. N. Schock, A. Adegbululge, J. Fenhann, I. Konstantinaviciute, W. Moomaw, H. B. Nimir, B. Schlamadinger, J. Torres-Martínez, C. Turner, Y. Uchiyama, S. J. V. Vuori, N. Wamukonya, and X Zhang, "Energy supply," in *Climate Change: Mitigation. Contribution of Working Group III to the Fourth Assessment Report of the Intergovernmental Panel on Climate Change*, B. Metz, O. R. Davidson, P. R. Bosch, R. Dave, and L. A. Meyer, Eds., Cambridge, UK: Cambridge Univer Press, 2007.
- [4] A. J. Ragauskas, K. W. Charlotte, B. H. Davison, G. Britovsek, J. Cairney, C. A. Eckert, W. J. Frederick, J. P. Hallett, D. J. Leak, C. L. Liotta, J. R. Mielenz, R. Murpgy, R. Templer, and T. Tschaplinski, "The path forward for biofuels and biomaterials," *Sci.*, vol. 311, pp. 484-489, 2006.
- [5] J. S. Tumuluru, C. T. Wright, J. R. Hess, and K. L. Kenney, "Review of biomass densification systems to develop uniform feedstock commodities for bioenergy application," *Biofuels Bioproc. Biorefin.*, vol. 5, pp. 683-707, 2011.
- [6] J. E. Hustad, Ø. Skreiberg, and O. K. Sønju, "Biomass combustion research and utilization in IEA countries," *Biomass Bioenergy*, vol., 9, pp. 235-255, 1995.
- [7] T. Brleka, L. Pezo, N. Voća, T. Krička, Đ. Vukmirović, and M. Bodroža-Solarov, "Chemometric approach for assessing the quality of olive cake pellets," *Fuel Process. Technol.* Vol., 116, pp. 250-256, 2013.
- [8] B. Lela, M. Barišić, and S. Nižetić, "Cardboard/sawdust briquettes as biomass fuel: Physical-mechanical and thermal characteristics," *Waste Manag.*, vol., 47, pp. 236-245, 2016.
- [9] S. Sokhansanj, S. Mani, X. Bi, P. Zaini, and L. G. Tabil, "Binderless pelletization of biomass," in *ASABE Annual International Meeting*, Tampa Convention Centre, Tampa, Florida, USA, 2005.
- [10] P. K. Adapa, G. J. Schoenau, L. G. Tabil, E. A. Arinze, A. K. Singh, and A. K. Dalai, "Customized and value-added high-quality alfalfa products: A new concept," *Agric. Eng. Internatl., The CIGR Ejournal*, vol., IX, pp. 1-28, 2007.
- [11] L. Tabil, P. Adapa, and M. Kshaninejad, "Biomass feedstock pre-processing – Part 2: Densification," *Biofuel Engineering Processing Technology*, M. A. Dos Santos Bernardes, Ed. InTech [online]. Available: <http://www.intechopen.com/books/biofuel-s-engineering-processtechnology/biomass-feedstock-pre-processing-part-2-densification>, (Accessed 15 July, 2016)
- [12] I. Obernberger, and G. Thek, "Physical characteristic and chemical composition of densified biomass fuels with regard to their combustion behaviour," *Biomass Bioenergy*, vol., 27, pp. 653-669, 2004.

- [13] N. Kaliyan, and R. Vance Morey, "Factors affecting strength and durability of densified biomass products," *Biomass Bioenergy*, vol., 33, pp. 337-359, 2009.
- [14] A. Demirbaş, "Effect of moisture and hydrogen content on the heating value of fuels," *Energy Sour., Part A: Recover., Utilization Environ. Eff.*, vol. 29, pp. 649-655, 2007. Available: <http://dx.doi.org/10.1080/009083190957801> (Assessed 15 November, 2017)
- [15] D. L. Klass, "Energy and synthetic fuels from biomass and wastes," *Handbook of energy technology and economics*, Wiley-Interscience, USA, 1983.
- [16] C. O. Adegoke, "A preliminary investigation of sawdust as high grade solid fuel," *Niger. J. Renew. Energy*, vol., 7, pp. 102-107, 1999.